



## Carbon isotopes in the marine biogeochemistry model FESOM2.1-REcoM3

Martin Butzin<sup>1,2</sup>, Ying Ye<sup>1</sup>, Christoph Völker<sup>1</sup>, Özgür Gürses<sup>1</sup>, Judith Hauck<sup>1</sup>, Peter Köhler<sup>1</sup>

<sup>1</sup>Alfred-Wegener-Institut Helmholtz-Zentrum für Polar- und Meeresforschung, D-27515 Bremerhaven, Germany

5

<sup>2</sup>Now at MARUM-Center for Marine Environmental Sciences, University of Bremen, D-28334 Bremen, Germany

*Correspondence to:* Martin Butzin (mbutzin@marum.de)

**Abstract.** In this paper we describe the implementation of the carbon isotopes <sup>13</sup>C and <sup>14</sup>C (radiocarbon) into the marine biogeochemistry model REcoM3. The implementation is tested in long-term equilibrium simulations where REcoM3 is coupled with the ocean general circulation model FESOM2.1, applying a low-resolution configuration and idealized climate forcing. Focusing on the carbon-isotopic composition of dissolved inorganic carbon ( $\delta^{13}\text{C}_{\text{DIC}}$  and  $\Delta^{14}\text{C}_{\text{DIC}}$ ), our model results are largely consistent with reconstructions for the pre-anthropogenic period. Our simulations also exhibit discrepancies, e.g., in upwelling regions and the interior of the North Pacific. Some of these differences are due to the limitations of our ocean circulation model setup which results in a rather shallow meridional overturning circulation. We additionally study the accuracy of two simplified modelling approaches for dissolved inorganic <sup>14</sup>C, which are faster (15 % and about a factor of five, respectively) than the complete consideration of the marine radiocarbon cycle. The accuracy of both simplified approaches is better than 5 % which should be sufficient for most studies of  $\Delta^{14}\text{C}_{\text{DIC}}$ .

10  
15  
20

## 1 Introduction

Carbon isotopes are powerful tools for tracing present and past biogeochemical cycles and water masses. The stable isotope carbon-13 (<sup>13</sup>C) can be used to study the anthropogenic perturbation of the global carbon cycle due to the combustion of isotopically depleted fossil fuels via the so-called <sup>13</sup>C Suess effect (e.g., Keeling 1979; Quay et al., 1992; Köhler 2016; Graven et al., 2021). Carbon-13 may also help to decipher the exchange between atmospheric, marine and terrestrial carbon reservoirs in the past, for example during the last glacial cycle (Köhler et al., 2006, Ciais et al., 2012, Broecker and McGee, 2013, Jeltsch-Thömmes et al., 2019, Menking et al., 2022). Furthermore, <sup>13</sup>C is a proxy for oceanic nutrients and can be employed to infer past marine biological productivity, export production, and water mass distributions assuming that calcareous tests of foraminifera are faithful recorders of dissolved inorganic <sup>13</sup>C (e.g., Broecker and Peng, 1982; Lynch-Stieglitz et al., 2007; Hesse et al., 2011; Schmittner et al. 2017). The radioactive isotope carbon-14 (radiocarbon, <sup>14</sup>C) is the most important geochemical

25  
30



chronometer for dating organic matter and for assessing ocean ventilation rates and pathways over the  
35 last 55000 years (Heaton et al., 2021; Rafter et al., 2022; Skinner and Bard, 2022, Skinner et al., 2023).  
In addition, the penetration of bomb-produced  $^{14}\text{C}$  into the oceans has provided a benchmark for ocean  
circulation models (Matsumoto et al., 2004). During the last decade, numerous ocean general circulation  
models have been equipped with carbon isotopes and applied in Earth system modelling studies (e.g.,  
Tschumi et al., 2011; Holden et al., 2013; Schmittner et al., 2013; Jahn et al., 2015; Menviel et al., 2015;  
40 Buchanan et al., 2019; Jeltsch-Thömmes et al., 2019; Dentith et al., 2020; Tjiputra et al., 2020; Claret et  
al., 2021; Liu et al. 2021; Morée et al., 2021).

Here, we describe the implementation of both carbon isotopes into the marine biogeochemistry model  
REcoM3 which is part of the AWI Earth System Model. The technical details will be described in Section  
2 and simulations in Section 3. Isotope results will be presented in terms of  $\delta^{13}\text{C}$  and  $\Delta^{14}\text{C}$  which express  
45 the relative deviations of observed  $^{13}\text{C}/^{12}\text{C}$  ( $^{13}R$ ) and  $^{14}\text{C}/^{12}\text{C}$  ( $^{14}R$ ) ratios with respect to specific standard  
values ( $^{13}R_{\text{std}} = 0.0112372$ ; Craig, 1957, and  $^{14}R_{\text{std}} = 1.176 \times 10^{-12}$ ; Karlén et al., 1964), where

$$\delta^{13}\text{C} = [^{13}R / ^{13}R_{\text{std}} - 1] \cdot 1000, \quad (1)$$

$$\delta^{14}\text{C} = [^{14}R / ^{14}R_{\text{std}} - 1] \cdot 1000, \quad (2)$$

and (following Stuiver and Pollach, 1977)

$$50 \quad \Delta^{14}\text{C} = \delta^{14}\text{C} - 2 (\delta^{13}\text{C} + 25 \text{‰}) (1 + \delta^{14}\text{C} / 1000). \quad (3)$$

Section 4 will conclude with a brief summary.

## 2 Model description

### 2.1 Short overview of REcoM3

The Regulated Ecosystem Model, version 3 (REcoM3) is described in detail by Gürses et al. (2023). Here,  
55 we will only give a brief summary of the common model features and describe the differences to the  
configuration that we use in this study. REcoM considers the marine biogeochemical cycles of carbon,  
nitrogen, silicon, iron, and oxygen. The ecosystem component of REcoM includes nutrients, two  
phytoplankton functional types (distinguishing between small phytoplankton and diatoms), one  
zooplankton functional type, one detritus type, and dissolved organic matter. Different to most other  
60 marine biogeochemistry models, REcoM does not rely on a fixed internal stoichiometry of phytoplankton.  
Instead, the composition of organic soft tissue is regulated (i.e., calculated) in response to light,  
temperature and nutrient supply which enables to assess stoichiometric shifts between present and past.  
The model includes a sediment layer in which sinking detritus (consisting of particulate organic matter,  
calcite and opal) is fully remineralized and where solutes are returned to the bottom water layer.  
65 Alternatively, REcoM3 can be run with the comprehensive sediment model MEDUSA2 (Munhoven,  
2021) which will be described in another paper (Ye et al., in prep.). Apart from the implementation of



carbon isotopes, the main difference to the standard REcoM3 configuration by Gürses et al. (2023) is that REcoM3 considers two zooplankton and two detritus groups instead of one, which would require to include six additional carbon-isotopic tracers at the expense of model speed. We refer to the configuration presented here as REcoM3p as an initial set-up for paleo studies. To simulate biogeochemical tracer circulation, REcoM3 needs a transport model. Here, we utilize the ocean general circulation model FESOM2.1 which is an update of FESOM2.0 (Danilov et al., 2017). The coupling of FESOM2.1 with REcoM3 is also described by Gürses et al. (2023), where all biogeochemical model equations except for carbon isotopes can be found.

75

## 2.2 Implementation of carbon isotopes

Carbon-13 and  $^{14}\text{C}$  are implemented as additional passive tracers, tripling the number of carbon-containing tracers in REcoM from 8 to 24. In the kinetic calculations of the carbonate system  $^{13}\text{C}$  and  $^{14}\text{C}$  are neglected because their abundances are small. For the same reason, and to ensure numerical stability in the other model calculations involving  $^{13}\text{C}$  and  $^{14}\text{C}$ , we do not apply the true values of the isotopic standard ratios but set  $^{13}R_{\text{std}} = 1$  and  $^{14}R_{\text{std}} = 1$  following Jahn et al. (2015). As a consequence,  $^{12}\text{C}$ ,  $^{13}\text{C}$ , and  $^{14}\text{C}$  concentrations are of the same magnitude but the scaling factors cancel out when  $^{13}\text{C}$  and  $^{14}\text{C}$  concentrations are converted to  $\delta^{13}\text{C}$  and  $\Delta^{14}\text{C}$  values. We consider isotopic fractionation during air-sea gas exchange, dissolution of  $\text{CO}_2$  in seawater, and photosynthesis by phytoplankton. In addition, the model accounts for radioactive decay and, optionally, cosmogenic production of  $^{14}\text{C}$ . The details are explained in the following subsections.

85

## 2.3 Carbon-13

### 2.3.1 Air-sea exchange

The isotopic fractionation during uptake and dissolution of  $^{13}\text{CO}_2$  is calculated according to Zhang et al. (1995), mostly following the biogeochemical protocol of the CMIP6 Ocean Model Intercomparison Project (OMIP-BGC protocol, Orr et al., 2017). That is, the air-sea exchange flux  $^{13}F$  is proportional to the difference between the saturation and in-situ concentrations of aqueous  $^{13}\text{CO}_2$ :

$$\begin{aligned} ^{13}F &= k_w ([^{13}\text{CO}_2^*]_{\text{sat}} - [^{13}\text{CO}_2^*]) \\ &= k_w (^{13}\alpha_k \ ^{13}\alpha_{\text{aq-g}} - 0.0002) (^{13}R_{\text{atm}} [\text{CO}_2^*]_{\text{sat}} - ^{13}R_{\text{DIC}} / ^{13}\alpha_{\text{DIC-g}} [\text{CO}_2^*]), \end{aligned} \quad (4)$$

95

where  $k_w$  is the  $\text{CO}_2$  gas transfer velocity (calculated according to Wanninkhof, 2014, additionally considering sea-ice cover), and  $[^{13}\text{CO}_2^*]_{\text{sat}}$  and  $[^{13}\text{CO}_2^*]$  are the saturation and in-situ concentrations of aqueous  $^{13}\text{CO}_2$ .  $^{13}R_{\text{atm}}$  and  $^{13}R_{\text{DIC}}$  are the  $^{13}\text{C}/^{12}\text{C}$  concentration ratios of atmospheric  $\text{CO}_2$  and dissolved inorganic carbon (DIC). Isotopic fractionation factors  $\alpha$  denote kinetic fractionation during  $\text{CO}_2$  gas



100 transfer ( $^{13}\alpha_k$ ), equilibrium fractionation during gas dissolution ( $^{13}\alpha_{\text{aq-g}}$ ), and equilibrium fractionation  
between DIC and gaseous  $\text{CO}_2$  ( $^{13}\alpha_{\text{DIC-g}}$ ). Numerical values were taken from Zhang et al. (1995) who  
measured kinetic and equilibrium fractionation of  $^{13}\text{C}$  in acidified freshwater. For kinetic fractionation  
we employ a constant value of  $^{13}\alpha_k = 0.99912$  which is the average between  $5\text{ }^\circ\text{C}$  ( $^{13}\alpha_k = 0.99919$ ) and  
21  $^\circ\text{C}$  ( $^{13}\alpha_k = 0.99905$ ). Equilibrium fractionation between aqueous and atmospheric  $^{13}\text{CO}_2$  is expressed  
105 as

$$^{13}\alpha_{\text{aq-g}} = 1 + 0.001 (0.0049 T - 1.31) \quad (5)$$

where  $T$  ( $^\circ\text{C}$ ) is the temperature of surface water. The numerical values of  $^{13}\alpha_k$  and  $^{13}\alpha_{\text{aq-g}}$  were determined  
for fresh water. To account for enhanced  $^{13}\text{C}$  fractionation in seawater associated with hydration reactions,  
equation (4) includes a correction factor of  $-0.0002$  following Zhang et al. (1995) which is not considered  
110 in the OMIP-BGC protocol. Fractionation between DIC and gaseous  $\text{CO}_2$  is calculated as

$$^{13}\alpha_{\text{DIC-g}} = 1 + 0.001 ((0.014 f\text{CO}_3 - 0.107) T + 10.53), \quad (6)$$

where  $f\text{CO}_3 = [\text{CO}_3^{2-}] / \text{DIC}$  is the carbonate fraction of DIC.

### 2.3.2 Biogenic fractionation

Photosynthesis of phytoplankton leads to isotopic depletion of particulate organic carbon (POC) which  
115 is expressed following Freeman and Hayes (1992):

$$[^{13}\text{C}_{\text{POC}}] = ^{13}R_{\text{POC}} [^{12}\text{C}_{\text{POC}}] = ^{13}R_{\text{aq}} / ^{13}\alpha_p [^{12}\text{C}_{\text{POC}}] \quad (7)$$

where  $[^{13}\text{C}_{\text{POC}}]$  and  $[^{12}\text{C}_{\text{POC}}]$  are the isotopic POC concentrations in phytoplankton,  $^{13}R_{\text{POC}}$  is the  
corresponding isotopic ratio,  $^{13}R_{\text{aq}}$  is the  $^{13}\text{C}/^{12}\text{C}$  concentration ratio of aqueous  $\text{CO}_2$ , and  $^{13}\alpha_p$  is the  
isotopic fractionation factor associated with photosynthesis. Various experimental and modelling studies  
120 have determined  $^{13}\alpha_p$  for certain phytoplankton species (Laws et al., 1995; Rau et al., 1996; Bidigare et  
al., 1997; Laws et al., 1997; Rau et al., 1997; Popp et al., 1998; Keller and Morel, 1999). However, it is  
uncertain to what extent these studies are globally representative and can be transferred into a single  
global modelling framework (see also the review by Brandenburg et al., 2022). Therefore, we pursue a  
less sophisticated but robust approach to calculate  $^{13}\alpha_p$  which has been inferred from a global dataset of  
125  $525\ \delta^{13}\text{C}_{\text{POC}}$  field measurements spanning the period 1962–2010 CE (Young et al., 2013):

$$^{13}\alpha_p = 1 + 0.001 (17.6 (1 - 2.02 / [\text{CO}_2^*])), \quad (8)$$

where  $[\text{CO}_2^*]$  is in  $\mu\text{mol L}^{-1}$ . Since no distinction is made between different phytoplankton species in  
equation (8), the carbon-isotopic composition of small phytoplankton and diatoms in our model is the  
same. Similarly to other models (e.g., Schmittner et al., 2013; Menviel et al., 2105; Buchanan et al., 2019;  
130 Tjiputra et al., 2020; Liu et al., 2021) we do not consider carbon-isotopic fractionation during formation  
and dissolution of biogenic calcite because the effect is small and varies between species ( $\alpha \sim 0.999$ – $1.003$   
according to Ziveri et al., 2003).



## 2.4 Radiocarbon

Radiocarbon is subject to radioactive decay, cosmogenic production, and isotopic fractionation. The  
135 radioactive decay (applying a half-life of 5700 years, Audi et al., 2003; Bé and Chechev, 2012; Kutschera,  
2013) is balanced in the model by cosmogenic  $^{14}\text{C}$  production fluxes or, alternatively, by prescribed  
atmospheric  $^{14}\text{CO}_2$  concentrations corresponding to atmospheric  $\Delta^{14}\text{C}$  values.

Fractionation factors are calculated analogously to  $^{13}\alpha$ , with  $^{14}\alpha = 2 \cdot ^{13}\alpha - 1$  (e.g., Craig, 1954). We have  
implemented  $^{14}\text{C}$  in two ways. The first approach (“CC”) considers the complete  $^{14}\text{C}$  cycle parallel to  $^{13}\text{C}$ .  
140 The second, approximate approach (“IC”) disregards isotopic fractionation of  $^{14}\text{C}$  and radioactive decay  
of organic matter. In turn,  $\text{DI}^{14}\text{C}$  and  $\text{DIC}$  have identical sources and sinks except for atmospheric  $\text{CO}_2$   
and radioactive decay. This “inorganic”  $^{14}\text{C}$  approach is conceptually similar, but not identical, to the  
“abiotic”  $^{14}\text{C}$  modelling approach described in the OMIP biogeochemical protocol (Orr et al., 2017). In  
our IC approach,  $\text{DIC}$  and  $\text{DI}^{14}\text{C}$  include biological sources and sinks. This does not apply to the OMIP-  
145 abiotic approach, which also considers alkalinity in a simplified way. In Section 3.3 we will scrutinize  
the accuracy of the IC approximation.

It has been shown that marine  $\Delta^{14}\text{C}$  values of  $\text{DIC}$  ( $\Delta^{14}\text{C}_{\text{DIC}}$ ) are primarily governed by transport and  
radioactive decay (Fiadeiro, 1982; see also Mouchet, 2013). This implies that  $\Delta^{14}\text{C}_{\text{DIC}}$  can be implemented  
into ocean general circulation models without a full carbon cycle model (cf. Toggweiler et al., 1989, and  
150 numerous other studies later on). We evaluate this  $\Delta^{14}\text{C}$  approximation (“DA”) in an additional simulation  
and compare it with REcoM approaches CC and IC also in Section 3.3.

A list of the various model experiments and their key features can be found in Table 1.

## 3 Results and discussions

### 155 3.1 Simulated ocean climatology

FESOM employs unstructured meshes with variable horizontal resolution. The default mesh of  
FESOM2.1-REcoM3 has about 127000 horizontal surface nodes (Gürses et al., 2023). Here, our model  
resolution is radically reduced, considering 3140 surface nodes corresponding to a median horizontal  
resolution of 260 km (the so-called pi-mesh, see Fig. A1 in Appendix A). This configuration requires  
160 fewer computational resources and allows to perform simulations over the time scale of marine carbon  
isotope equilibration (i.e. over several thousand years) within a few weeks. Vertical resolution is 47 layers  
using  $z^*$  coordinates with nonlinear free surface (further details see Scholz et al., 2019).

In a first step we run FESOM without REcoM over 1000 years to spinup the overturning circulation and  
thermohaline fields. FESOM was initialized with seasonal winter temperatures and salinities by Steele et  
165 al. (2001), and driven with annually repeated atmospheric fields using Corrected Normal Year Forcing  
Version 2.0 (Large and Yeager, 2009; for an overview see also Griffies et al., 2012). As FESOM2.1 had



originally been adjusted for higher resolution and different forcing, we retuned the model in our setup by reducing the maximum Gent-McWilliams thickness diffusivity from originally  $2000 \text{ m}^2 \text{ s}^{-1}$  to  $1000 \text{ m}^2 \text{ s}^{-1}$ . After 1000 simulated years there was no significant drift of thermohaline and circulation  
170 fields, REcoM3p was turned on, and both models were run over additional 5000 years. REcoM3p was initialized with gridded concentration fields of total alkalinity, DIC and nitrate from GLODAPv2 (Key et al., 2015; Lauvset et al., 2016), oxygen and silicate from WOA13 (Garcia et al., 2014a, 2014b), and dissolved iron according to Aumont et al. (2003) and Tagliabue et al. (2012). Dissolved inorganic  $^{13}\text{C}$  and  $^{14}\text{C}$  were initialized with DIC, assuming initial fractionation values of  $\delta^{13}\text{C}_{\text{DIC}} = 0 \text{ ‰}$  and  $\Delta^{14}\text{C}_{\text{DIC}} = -150 \text{ ‰}$ , respectively. REcoM3p was forced with constant atmospheric  $\text{CO}_2$  concentrations ( $[\text{CO}_2]_{\text{atm}} = 284.3 \text{ ppmv}$ ;  $[\text{CO}_2]_{\text{atm}}$  and  $[\text{CO}_2]_{\text{atm}}$  corresponding to  $\delta^{13}\text{C}_{\text{atm}} = -6.61 \text{ ‰}$  and  $\Delta^{14}\text{C}_{\text{atm}} = 0 \text{ ‰}$ , respectively, following Orr et al., 2017), and with climatological-mean monthly fluxes of aeolian iron deposition (Albani et al., 2014).

As discussed in the following, our low-resolution test setup sufficiently captures the basic thermohaline  
180 circulation structures obtained with FESOM2.0 in higher-resolution simulations (Scholz et al., 2019, 2022). Compared to observations, our simulations exhibit a warm bias for thermocline and intermediate water as well as for North Atlantic Deep Water (NADW; see Fig. A2 in Appendix A). The most notable exception is the region of the North Atlantic Gulf stream which is not properly resolved and where upper ocean temperatures are considerably underestimated. The temperature biases covary with salinity biases.  
185 That is, simulated salinities are also higher than observations where simulated temperatures are high, and salinities are too low where simulated temperatures tend to be low (Fig. A3). In the Atlantic, FESOM arrives at a maximum meridional overturning circulation (AMOC) of about  $16 \text{ Sv}$  ( $1 \text{ Sv} = 1 \times 10^6 \text{ m}^3 \text{ s}^{-1}$ , Fig. A4), which is at the lower bound of observations while the simulated overturning cell is too shallow compared to observational estimates (see Buckley and Marshall, 2016; and further references therein).  
190 For the purposes of this study, our simulations also reasonably reflect the observed large-scale pattern of DIC (Key et al., 2015; Lauvset et al., 2016). That is, low concentrations are found at upper levels of the subtropical oceans and in the freshly ventilated interior of the North Atlantic, while DIC concentrations progressively increase in the South Atlantic and in the deep North Pacific (Fig. A5).

### 3.2 Carbon-13

195 We now focus on the carbon-isotopic composition of DIC near the sea surface and along meridional sections through the Atlantic and Pacific. Regarding  $\delta^{13}\text{C}_{\text{DIC}}$ , we compare our model results with the gridded preindustrial (PI)  $\delta^{13}\text{C}_{\text{DIC}}$  climatology by Eide et al. (2017). Their reconstruction does not consider the upper 200 m to exclude the  $^{13}\text{C}$  Suess effect.

In wide areas, our simulated near-surface  $\delta^{13}\text{C}_{\text{DIC}}$  values are in the range of 1 to 2 ‰ (Fig. 1a). Higher  
200  $\delta^{13}\text{C}_{\text{DIC}}$  values are simulated in the subtropical oceans, particularly in the Atlantic, southeast Pacific and southern Indian Ocean. Isotopic depletion of up to  $\sim -1 \text{ ‰}$  is found in the eastern equatorial Pacific, the



subpolar North Pacific, the Bay of Bengal, and in the Angola Basin. While our simulation captures the reconstructed spatial pattern (shown in Fig. 1b), the simulated range of  $\delta^{13}\text{C}_{\text{DIC}}$  variations is larger than in the reconstruction. That is, the model results are too high in the lower latitudes and too low in the above mentioned depletion regions (Fig. 2a).

Considering the interior of the Atlantic Ocean, our simulation yields higher  $\delta^{13}\text{C}_{\text{DIC}}$  in the North Atlantic than in the South Atlantic, and small vertical  $\delta^{13}\text{C}_{\text{DIC}}$  gradients in the high latitudes of both hemispheres (Fig. 1c). In the Pacific, our simulation displays a reversed meridional  $\delta^{13}\text{C}_{\text{DIC}}$  gradient with the strongest isotopic depletion at intermediate depths in the North Pacific. Our results are roughly in line with the reconstruction by Eide et al. (2017, cf. Fig. 1d) but overestimate  $\delta^{13}\text{C}_{\text{DIC}}$  in the upper Pacific at low latitudes as well as in the North Pacific between 1.5 km and 3 km depth (Fig. 2b). Similar inaccuracies are seen in other models (Tagliabue and Bopp, 2008; Schmittner et al., 2013; Jahn et al., 2015; Buchanan et al., 2019; Jeltsch-Thömmes et al., 2019; Dentith et al., 2020; Tjiputra et al., 2020; Liu et al., 2021).

To some extent, the differences between simulated and observed  $\delta^{13}\text{C}_{\text{DIC}}$  ( $\Delta\delta^{13}\text{C}_{\text{DIC}}$ ) can be attributed by decomposing  $\delta^{13}\text{C}_{\text{DIC}}$  into biologic and thermodynamic sources,

$$\delta^{13}\text{C}_{\text{DIC}} = \delta^{13}\text{C}_{\text{BIO}} + \delta^{13}\text{C}_{\text{AS}}, \quad (9)$$

where  $\delta^{13}\text{C}_{\text{BIO}}$  specifies the imprint of isotopic fractionation, respiration and remineralization of organic matter in the absence of air-sea exchange. Following Broecker and Maier-Reimer (1992),  $\delta^{13}\text{C}_{\text{BIO}}$  is frequently determined from the covariation of  $\delta^{13}\text{C}_{\text{DIC}}$  with marine phosphate ( $\text{PO}_4^{3-}$ ). We adopt this approach, employing revised parameter values by Eide et al. (2017) and tentatively replacing  $\text{PO}_4^{3-}$  with dissolved inorganic nitrogen (DIN) divided by 16 because  $\text{PO}_4^{3-}$  is not considered by REcoM3p,

$$\delta^{13}\text{C}_{\text{BIO}} = (2.8 - 1.1 \text{ PO}_4^{3-}) \text{‰} \equiv (2.8 - 0.069 \text{ DIN}) \text{‰}, \quad (10)$$

where  $\text{PO}_4^{3-}$  and DIN are in  $\mu\text{mol kg}^{-1}$ . The thermodynamic component  $\delta^{13}\text{C}_{\text{AS}}$  describes the effects of air-sea exchange and ocean circulation and is the residual of observed  $\delta^{13}\text{C}_{\text{DIC}}$  and reconstructed  $\delta^{13}\text{C}_{\text{BIO}}$ .

In the following we compare  $\Delta\delta^{13}\text{C}_{\text{DIC}}$  with the differences between the simulated and reconstructed  $\delta^{13}\text{C}_{\text{DIC}}$  components,  $\Delta\delta^{13}\text{C}_{\text{BIO}}$  and  $\Delta\delta^{13}\text{C}_{\text{AS}}$ . It appears that  $\Delta\delta^{13}\text{C}_{\text{DIC}}$  corresponds to  $\Delta\delta^{13}\text{C}_{\text{BIO}}$  in the low latitudes, upwelling regions, and the interior of the Atlantic (cf. Figs. 2 and 3), which points to model deficiencies in describing the sinking and regeneration of  $^{13}\text{C}$ -depleted organic carbon. On the other hand,  $\Delta\delta^{13}\text{C}_{\text{DIC}}$  corresponds to  $\Delta\delta^{13}\text{C}_{\text{AS}}$  in the upper thermocline of the open oceans in the Southern hemisphere (shown in Fig. 4). While our results may generally suffer from the coarse model resolution and simplified climate forcing, the specific reasons for this correspondence are not obvious. As a residual term  $\delta^{13}\text{C}_{\text{AS}}$  may also reflect effects of biological  $^{13}\text{C}$  cycling which are not captured by Equation (10). For example,  $\delta^{13}\text{C}_{\text{BIO}}$  is estimated for constant isotopic fractionation of marine organic matter of -19 ‰ while  $\delta^{13}\text{C}_{\text{POC}}$  varies by about 10 ‰ according to field data (Verwega et al., 2021; see also Fig. 6a).





235 Therefore, we explore the sensitivity of  $\delta^{13}\text{C}_{\text{DIC}}$  to biogenic fractionation in an additional experiment (“NP”) in which biogenic fractionation is disabled (i.e.,  $^{13}\alpha_p = 1$  in equation (8)). Compared to the default simulation,  $\delta^{13}\text{C}_{\text{DIC|NP}}$  decreases by up to 1 ‰ in the pelagic euphotic zone while  $\delta^{13}\text{C}_{\text{DIC|NP}}$  increases in the dysphotic zone below, which is particularly the case in highly productive regions (Fig. 5a-b). In the aphotic interior of the ocean  $\delta^{13}\text{C}_{\text{DIC|NP}}$  progressively increases from the North Atlantic towards the North  
240 Pacific by up to 2.4 ‰ (Fig. 5c). These findings are in line with similar sensitivity studies (Schmittner et al., 2013; Dentith et al., 2020) as well as with simulations comparing different parametrizations for  $^{13}\alpha_p$  (Jahn et al., 2015; Buchanan et al., 2019; Dentith et al., 2020; Liu et al., 2021).

Our default simulation with enabled photosynthetic fractionation yields  $\delta^{13}\text{C}_{\text{POC}}$  values between -18 and -25 ‰ while observations from the last decades range from -15 to -35 ‰ (Verwega et al., 2021; Fig. 6a).  
245 The model overestimates  $\delta^{13}\text{C}_{\text{POC}}$  at most locations (Fig. 6b). According to sensitivity experiment NP, the overestimation of  $\delta^{13}\text{C}_{\text{POC}}$  should result in overly enriched  $\delta^{13}\text{C}_{\text{DIC}}$  in the twilight and dark zones of highly productive regions (Fig. 5b) while Figure 2a indicates that the opposite is the case. However, this is only an apparent contradiction because the  $\delta^{13}\text{C}_{\text{POC}}$  observations are biased by the  $^{13}\text{C}$  Suess effect. Moreover, they exhibit a negative trend (by -3 ‰ between 1960 and 2010) which is about twice as high  
250 as the known  $^{13}\text{C}$  Suess effect on aqueous  $\text{CO}_2$  (Young et al., 2013; Verwega et al., 2021). It has been presumed that this trend also reflects a shift in phytoplankton species composition (Lorrain et al., 2020; Verwega et al., 2021). Both effects are not considered in our simulation. A conclusive analysis would require transient simulations including historical values of atmospheric  $^{13}\text{CO}_2$ .

### 3.3 Radiocarbon

255 We consider  $\Delta^{14}\text{C}_{\text{DIC}}$  and compare our model results with gridded fields of pre-bomb  $\Delta^{14}\text{C}_{\text{DIC}}$  provided by the Global Ocean Data Analysis Project (GLODAPv1.1, Key et al., 2004).

In the comprehensive radiocarbon cycle simulation (CC)  $\Delta^{14}\text{C}_{\text{DIC|CC}}$  is in the range of -40 to -140 ‰ (average value: -65 ‰) near the surface (at 50 m), with the highest values in the subtropical gyres and the lowest values in the Southern Ocean (Fig. 7a). In the interior of the Atlantic,  $\Delta^{14}\text{C}_{\text{DIC|CC}}$  ranges between  
260 -70 and -170 ‰ and decreases from the surface to the bottom, with small vertical gradients in the high latitudes (Fig. 8a). This is superimposed by a southward gradient of  $\Delta^{14}\text{C}_{\text{DIC}}$ . The meridional  $\Delta^{14}\text{C}_{\text{DIC}}$  gradient reverses in the Pacific. Different to the northern North Atlantic, there is no evidence of deep sea ventilation in the North Pacific where our model arrives at minimum  $\Delta^{14}\text{C}_{\text{DIC|CC}}$  values exceeding -290 ‰ (Fig. 8a).

265 Overall, simulation CC captures the large-scale distribution of pre-nuclear  $\Delta^{14}\text{C}_{\text{DIC}}$  as reconstructed by GLODAPv1.1 (Fig. 7a-b, 8a-b). However, at 50 m depth the simulated  $\Delta^{14}\text{C}_{\text{DIC}}$  is too high by 10 – 30 ‰ in the low- and mid-latitudes, and too low by about the same amount in the high latitudes (see Fig. 9a; according to GLODAP  $\Delta^{14}\text{C}_{\text{DIC}}$  ranges from -50 to -170 ‰ with -71 ‰ on average). In the interior of the oceans, our model results are typically 20 – 60 ‰ too low (Fig. 10). The excessive depletion reaches





270 -70 ‰ in the abyssal North Atlantic and in the North Pacific at 3 km depth (Fig. 10a). In the upper layers of the oceans, the GLODAPv1.1 data probably reflect the  $^{14}\text{C}$  Suess effect (Suess, 1955), which is not considered in our simulations. The excessive depletion in the deep sea indicates that the simulated AMOC leads to overly shallow and weak ocean ventilation, which is enhanced by the progressive radioactive decay of  $\text{DI}^{14}\text{C}$  along its passage through the interior of the ocean.

275 Different to  $\delta^{14}\text{C}_{\text{DIC}}$ ,  $\Delta^{14}\text{C}_{\text{DIC}}$  is corrected for isotopic fractionation. In practice (as well as in the comprehensive  $\text{DI}^{14}\text{C}$  cycle modelling approach CC), the correction is made after the simultaneous determination of  $\delta^{13}\text{C}_{\text{DIC}}$  and  $\delta^{14}\text{C}_{\text{DIC}}$ . In the inorganic  $^{14}\text{C}$  (IC) modelling approach the fractionation of  $^{14}\text{C}$  is omitted beforehand, so that posterior corrections are not necessary. That is,  $\delta^{14}\text{C}_{\text{DIC|IC}}$  equals  $\Delta^{14}\text{C}_{\text{DIC|IC}}$  which should equal  $\Delta^{14}\text{C}_{\text{DIC|CC}}$ . As the IC approach also neglects the radioactive decay of  
280 organic carbon, it considers seven tracers less than the CC approach which is accompanied by an increase in model speed (simulated years per day) of about 15 %.

At 50 m depth  $\Delta^{14}\text{C}_{\text{DIC|IC}}$  ranges from -50 ‰ to -160 ‰ with an average value of 72 ‰ (Fig. 7c). Similar to experiment CC, the highest values of  $\Delta^{14}\text{C}_{\text{DIC|IC}}$  are found in subtropical surface waters. The lowest surface water values of  $\Delta^{14}\text{C}_{\text{DIC|IC}}$  are also found in the Southern Ocean. In the interior of the oceans, the  
285 isotopic depletion with respect to the atmosphere ranges from -90 ‰ in the North Atlantic to -310 ‰ in the North Pacific (Fig 8c). Comparing IC with the GLODAPv1.1 reconstruction, we find that the enrichment of subtropical surface values is less pronounced in IC while the depletion in the high-latitudes increases (Fig. 9b). The latter is also the case in the interior of the oceans (Fig. 10b). Most notably, the outcomes of experiment IC are everywhere lower (by up to 30 ‰) than the results of simulation CC (Figs.  
290 11a, 11c) which is explained as follows.

Analogously to sensitivity experiment NP, the IC approach disregards photosynthetic fractionation which leads to lower  $\text{DI}^{14}\text{C}$  concentrations in the euphotic zone than in simulation CC. In addition, the IC approach disregards the  $\text{DI}^{14}\text{C}$  enrichment of the mixed layer associated with air-sea exchange. Furthermore, since the IC approach disregards the radioactive decay of phytoplankton, the loss of  $\text{DI}^{14}\text{C}$   
295 due to photosynthesis is overestimated in the mixed layer. Therefore, preformed  $\text{DI}^{14}\text{C}$  is systematically lower than in simulation CC and becomes further depleted through radioactive decay in the deep sea. This bias is similar to the lower values of “abiotic”  $\Delta^{14}\text{C}$  compared to “biotic”  $\Delta^{14}\text{C}$  simulated by Frischknecht et al. (2022).

Instead of computing absolute concentrations of DIC,  $\text{DI}^{13}\text{C}$ , and  $\text{DI}^{14}\text{C}$  and converting them to  $\Delta^{14}\text{C}_{\text{DIC}}$   
300 a posteriori, the  $\Delta^{14}\text{C}$  approximation (DA) simulates  $^{14}R_{\text{DIC|DA}} = 1 + 0.001 \Delta^{14}\text{C}_{\text{DIC|DA}}$  as a single radioconservative tracer which is connected with the carbon cycle through the  $^{14}\text{CO}_2$  air-sea exchange. This approach is about five times faster than the approaches CC and IC. First results of the implementation of  $^{14}R_{\text{DIC|DA}}$  into FESOM2 were shown by Lohmann et al. (2020) for the default FESOM mesh with 127000 horizontal surface nodes. Here, we repeated the experiment, now using the low-resolution mesh  
305 of experiments CC and IC to be able to compare the results of all approaches directly. For the same reason,



we discuss model results after 5000 simulated years but point out that experiment DA has been run over 17000 years in total. The maximum drift of  $\Delta^{14}\text{C}_{\text{DIC|DA}}$  between 5000 and 17000 simulated years is about -3.5 ‰ in North Pacific Deep Water, which is much smaller than the  $\Delta^{14}\text{C}_{\text{DIC}}$  differences between the various modelling approaches in this study after 5000 years shown below.

- 310 At 50 m depth  $\Delta^{14}\text{C}_{\text{DIC|DA}}$  ranges from -40 to -130 ‰, with  $\Delta^{14}\text{C}_{\text{DIC|DA}} = -58$  ‰ on average (Fig. 7d). In intermediate and deep water  $\Delta^{14}\text{C}_{\text{DIC|DA}}$  declines from -60 ‰ in the North Atlantic to -280 ‰ in the North Pacific (Fig. 8d). At upper levels,  $\Delta^{14}\text{C}_{\text{DIC|DA}}$  is almost everywhere higher than  $\Delta^{14}\text{C}_{\text{DIC}}$  according to GLODAPv1.1 (Figs. 9c, 10c). In the deep sea,  $\Delta^{14}\text{C}_{\text{DIC|DA}}$  is still too low but the depletion is less pronounced than in simulations CC and IC (Fig. 10c).
- 315 Experiment DA yields the highest  $\Delta^{14}\text{C}_{\text{DIC}}$  values of all the three modelling approaches (Fig. 11). The DA approach assumes that DIC concentrations are constant and homogeneous (for a rigorous treatise see Mouchet, 2013). Following Toggweiler et al. (1989), our calculation of  $^{14}\text{CO}_2$  air-sea exchange fluxes in simulation DA assumes a DIC concentration of 2000  $\text{mmol m}^{-3}$  in the mixed layer which is somewhat lower than observed and simulated in most areas, most notably in the high latitudes (Fig. A5a-b). This
- 320 leads to faster and hence higher  $^{14}\text{C}$  uptake in DA than in CC and IC because the  $^{14}\text{CO}_2$  invasion flux is inversely proportional to the DIC concentration in the mixed layer. The absolute  $\Delta^{14}\text{C}_{\text{DIC}}$  differences between DA and CC are largely less than 10 ‰ (Figs. 11b, 11d). Moreover, the relative uncertainty of the DA approach with respect to the correct  $\text{DI}^{14}\text{C}$  implementation is less than 5 % (Fig. 12) and actually smaller than the error of 10 % originally estimated by Fiadeiro (1982).

## 325 4 Summary

We have added the carbon isotopes  $^{13}\text{C}$  and  $^{14}\text{C}$  to the marine biogeochemistry model REcoM3 and tested the implementation in long-term equilibrium simulations in which the configuration REcoM3p was coupled with the ocean general circulation model FESOM2.1. Regarding the carbon-isotopic composition of DIC ( $\delta^{13}\text{C}_{\text{DIC}}$  and  $\Delta^{14}\text{C}_{\text{DIC}}$ ), our model results are largely consistent with marine  $\delta^{13}\text{C}_{\text{DIC}}$  and  $\Delta^{14}\text{C}_{\text{DIC}}$

330 fields reconstructed for the pre-anthropogenic period. The simulations also exhibit discrepancies, such as overly depleted  $\delta^{13}\text{C}_{\text{DIC}}$  values in upwelling regions and excessive depletion of  $\Delta^{14}\text{C}_{\text{DIC}}$  in the interior of the North Pacific. To some extent, the inaccuracies of  $\delta^{13}\text{C}_{\text{DIC}}$  indicate shortcomings in modelled organic carbon cycling. The radiocarbon results ( $\Delta^{14}\text{C}_{\text{DIC}}$ ) reflect the rather shallow overturning circulation provided by our low-resolution ocean general circulation model test configuration with idealized repeat

335 year climate forcing. As future simulations with a scientific focus will be carried out with considerably higher horizontal resolution and more realistic climate forcing, we expect some of the biases discussed in this study to decrease. These simulations should also consider transient boundary conditions of  $^{13}\text{C}$  and  $^{14}\text{C}$  which provide additional benchmarks for the model. For these reasons we did not attempt to further



tune REcoM3p here, e.g. by adjusting semi-empirical biogeochemical parameters such as gas transfer  
340 velocity or biogenic fractionation coefficients.

As  $\Delta^{14}\text{C}_{\text{DIC}}$  is dominated by radioactive decay and transport processes, we have additionally explored the  
accuracy of two simplified modelling approaches which are more efficient than the complete  
consideration (CC) of the  $\text{DI}^{14}\text{C}$  cycle. One approach (IC) neglects isotopic fractionation but still  
considers biological processes. Another approach (DA) only considers the  $\text{DI}^{14}\text{C} / \text{DIC}$  ratio for constant  
345 and homogeneous DIC concentrations and further disregards the marine carbon cycle. The relative  
uncertainty between the comprehensive and simplified approaches is less than 5 %. Therefore, the  
simplified  $\Delta^{14}\text{C}_{\text{DIC}}$  modelling approaches should be sufficiently accurate for radiocarbon dating of marine  
climate archives.

350 *Code availability.* The source code is available at <https://doi.org/10.5281/zenodo.8169243>.

*Author contributions.* MB developed the isotope code, conducted the simulations and prepared the  
manuscript with contributions from all co-authors.

355 *Competing interest.* The authors declare that they have no conflict of interest.

*Acknowledgements.* This work was supported by the German Federal Ministry of Education and Research  
(BMBF) through the PalMod project (grant number: 01LP1919A) which is part of the Research for  
Sustainability initiative FONA (<https://www.fona.de>). MB is additionally funded through DFG-ANR  
360 project MARCARA. JH and OG were funded by the Initiative and Networking Fund of the Helmholtz  
Association (Helmholtz Young Investigator Group Marine Carbon and Ecosystem Feedbacks in the Earth  
System [MarESys], grant number VH-NG-1301). We thank D. Sidorenko for FESOM model support.



## References

- 365 Albani, S., Mahowald, N. M., Perry, A. T., Scanza, R. A., Zender, C. S., Heavens, N. G., Maggi, V., Kok, J. F., and Otto-Bliesner, B. L.: Improved dust representation in the Community Atmosphere Model, *Journal of Advancements in Modeling Earth Systems*, 6, 541–570, <https://doi.org/10.1002/2013MS000279>, 2014.
- Antonov, J. I., Seidov, D., Boyer, T. P., Locarnini, R. A., Mishonov, A. V., and Garcia, H. E.: World  
370 Ocean Atlas 2009, Volume 2: Salinity, Washington, D.C., 2010.
- Audi, G., Bersillon, O., Blachot, J., and Wapstra, A. H.: The Nubase evaluation of nuclear and decay properties, *Nuclear Physics A*, 729, 3–128, <https://doi.org/10.1016/j.nuclphysa.2003.11.001>, 2003.
- Aumont, O., Maier-Reimer, E., Blain, S., and Monfray, P.: An ecosystem model of the global ocean including Fe, Si, P colimitations, *Global Biogeochemical Cycles*, 17, 1060,  
375 <https://doi.org/10.1029/2001GB001745>, 2003.
- Bé, M.-M. and Chechev, V. P.:  $^{14}\text{C}$  - Comments on evaluation of decay data, Laboratoire National Henri Becquerel, Gif-sur-Yvette, [http://www.lnhb.fr/nuclides/C-14\\_com.pdf](http://www.lnhb.fr/nuclides/C-14_com.pdf), 2012.
- Bidigare, R. R., Fluegge, A., Freeman, K. H., Hanson, K. L., Hayes, J. M., Hollander, D., Jasper, J. P., King, L. L., Laws, E. A., Milder, J., Millero, F. J., Pancost, R., Popp, B. N., Steinberg, P. A., and  
380 Wakeham, S. G.: Consistent fractionation of  $^{13}\text{C}$  in nature and in the laboratory: Growth-rate effects in some haptophyte algae, *Global Biogeochemical Cycles*, 11, 279–292, <https://doi.org/10.1029/96GB03939>, 1997.
- Brandenburg, K. M., Rost, B., de Waal, D. B. V., Hoins, M., and Sluijs, A.: Physiological control on carbon fractionation in marine phytoplankton, *Biogeosciences*, 19, 3305–3315,  
385 <https://doi.org/10.5194/bg-19-3305-2022>, 2022.
- Broecker, W. S. and McGee, D.: The  $^{13}\text{C}$  record for atmospheric  $\text{CO}_2$ : What is it trying to tell us?, *Earth and Planetary Science Letters*, 368, 175–182, <https://doi.org/10.1016/j.epsl.2013.02.029>, 2013.
- Broecker, W. S. and Maier-Reimer, E.: The influence of air and sea exchange on the carbon isotope distribution in the sea, *Global Biogeochemical Cycles*, 6, 315–320,  
390 <https://doi.org/10.1029/92GB01672>, 1992.
- Buchanan, P. J., Matear, R. J., Chase, Z., Phipps, S. J., and Bindoff, N. L.: Ocean carbon and nitrogen isotopes in CSIRO Mk3L-COAL version 1.0: a tool for palaeoceanographic research, *Geoscientific Model Development*, 12, 1491–1523, <https://doi.org/10.5194/gmd-12-1491-2019>, 2019.



- Buckley, M. W. and Marshall, J.: Observations, inferences, and mechanisms of the Atlantic Meridional  
395 Overturning Circulation: A review, *Reviews of Geophysics*, 54, 2015RG000493,  
<https://doi.org/10.1002/2015RG000493>, 2016.
- Ciais, P., Tagliabue, A., Cuntz, M., Bopp, L., Scholze, M., Hoffmann, G., Lourantou, A., Harrison, S.P.,  
Prentice, I.C., Kelley, D.I., Koven, C.D., Piao, S. Large inert carbon pool in the terrestrial biosphere  
during the Last Glacial Maximum. *Nature Geoscience* 5, 74–79, <https://doi.org/10.1038/ngeo1324>,  
400 2012.
- Claret, M., Sonnerup, R. E., and Quay, P. D.: A Next Generation Ocean Carbon Isotope Model for Climate  
Studies I: Steady State Controls on Ocean  $^{13}\text{C}$ , *Global Biogeochemical Cycles*, 35, e2020GB006757,  
<https://doi.org/10.1029/2020GB006757>, 2021.
- Craig, H.: Carbon 13 in plants and the relationships between carbon 13 and carbon 14 variations in nature,  
405 *The Journal of Geology*, 62, 115–149, 1954.
- Craig, H.: Isotopic standards for carbon and oxygen and correction factors for mass-spectrometric  
analysis of carbon dioxide, *Geochimica et Cosmochimica Acta*, 12, 133–149,  
[https://doi.org/10.1016/0016-7037\(57\)90024-8](https://doi.org/10.1016/0016-7037(57)90024-8), 1957.
- Danilov, S., Sidorenko, D., Wang, Q., and Jung, T.: The Finite-volume Sea ice–Ocean Model (FESOM2),  
410 *Geoscientific Model Development*, 10, 765–789, <https://doi.org/10.5194/gmd-10-765-2017>, 2017.
- Dentith, J. E., Ivanovic, R. F., Gregoire, L. J., Tindall, J. C., and Robinson, L. F.: Simulating stable carbon  
isotopes in the ocean component of the FAMOUS general circulation model with MOSES1 (XOAVI),  
*Geoscientific Model Development*, 13, 3529–3552, <https://doi.org/10.5194/gmd-13-3529-2020>, 2020.
- Eide, M., Olsen, A., Ninnemann, U. S., and Johannessen, T.: A global ocean climatology of preindustrial  
415 and modern ocean  $\delta^{13}\text{C}$ , *Global Biogeochemical Cycles*, 2016GB005473,  
<https://doi.org/10.1002/2016GB005473>, 2017.
- Fiadeiro, M. E.: Three-dimensional modeling of tracers in the deep Pacific Ocean, II. Radiocarbon and  
the circulation, *Journal of Marine Research*, 40, 537–550, 1982
- Freeman, K. H. and Hayes, J. M.: Fractionation of carbon isotopes by phytoplankton and estimates of  
420 ancient CO<sub>2</sub> levels, *Global Biogeochemical Cycles*, 6, 185–198, <https://doi.org/10.1029/92GB00190>,  
1992.
- Frischknecht, T., Ekici, A., and Joos, F.: Radiocarbon in the land and ocean components of the  
Community Earth System Model. *Global Biogeochemical Cycles*, 36, e2021GB007042, <https://doi.org/10.1029/2021GB007042>, 2022.



- 425 Garcia, H. E., Locarnini, R. A., Boyer, T. P., Antonov, J. I., Baranova, O. K., Zweng, M. M., Reagan, J. R., and Johnson, D. R.: World Ocean Atlas 2013, Volume 3: Dissolved Oxygen, Apparent Oxygen Utilization, and Oxygen Saturation, 2014a.
- Garcia, H. E., Locarnini, R. A., Boyer, T. P., Antonov, J. I., Baranova, O. K., Zweng, M. M., Reagan, J. R., and Johnson, D. R.: World Ocean Atlas 2013, Volume 4: Dissolved Inorganic Nutrients (phosphate, 430 nitrate, silicate), 2014b.
- Graven, H., Lamb, E., Blake, D., and Khatiwala, S.: Future Changes in  $\delta^{13}\text{C}$  of Dissolved Inorganic Carbon in the Ocean, *Earth's Future*, 9, e2021EF002173, <https://doi.org/10.1029/2021EF002173>, 2021.
- Griffies, S. M., Winton, M., Samuels, B., Danabasoglu, G., Yeager, S., Marsland, S., Drange, H., and 435 Bentsen, M.: Datasets and protocol for the CLIVAR WGOMD Coordinated Ocean-sea ice Reference Experiments (COREs), WCRP Report No. 21/2012, <https://eprints.soton.ac.uk/350257>, 2012.
- Gürses, Ö., Oziel, L., Karakus, O., Sidorenko, D., Völker, C., Ye, Y., Zeising, M., and Hauck, J.: Ocean biogeochemistry in the coupled ocean-sea ice-biogeochemistry model FESOM2.1-REcoM3, *Geoscientific Model Development Discussions* [preprint], <https://doi.org/10.5194/gmd-2023-2>, in 440 press, 2023.
- Heaton, T. J., Bard, E., Bronk Ramsey, C., Butzin, M., Köhler, P., Muscheler, R., Reimer, P. J., and Wacker, L.: Radiocarbon: A key tracer for studying Earth's dynamo, climate system, carbon cycle, and Sun, *Science*, 374, eabd7096, <https://doi.org/10.1126/science.abd7096>, 2021.
- Hesse, T., Butzin, M., Bickert, T., and Lohmann, G.: A model-data comparison of  $\delta^{13}\text{C}$  in the glacial 445 Atlantic Ocean, *Paleoceanography*, 26, PA3220, <https://doi.org/10.1029/2010PA002085>, 2011.
- Holden, P. B., Edwards, N. R., Müller, S. A., Oliver, K. I. C., Death, R. M., and Ridgwell, A.: Controls on the spatial distribution of oceanic  $\delta^{13}\text{C}_{\text{DIC}}$ , *Biogeosciences*, 10, 1815–1833, <https://doi.org/10.5194/bg-10-1815-2013>, 2013.
- Jahn, A., Lindsay, K., Giraud, X., Gruber, N., Otto-Bliesner, B. L., Liu, Z., and Brady, E. C.: Carbon 450 isotopes in the ocean model of the Community Earth System Model (CESM1), *Geoscientific Model Development*, 8, 2419–2434, <https://doi.org/10.5194/gmd-8-2419-2015>, 2015.
- Jeltsch-Thömmes, A., Battaglia, G., Cartapanis, O., Jaccard, S. L., and Joos, F.: Low terrestrial carbon storage at the Last Glacial Maximum: constraints from multi-proxy data, *Climate of the Past*, 15, 849–879, <https://doi.org/10.5194/cp-15-849-2019>, 2019.
- 455 Karlén, I., Olsson, I. U., Källberg, P.W., and Kilicci, S.: Absolute determination of the activity of two  $\text{C}^{14}$  dating standards, *Arkiv för Geofysik*, 4, 465–471, 1964.



- Keeling, C. D.: The Suess effect: <sup>13</sup>Carbon-<sup>14</sup>Carbon interrelations, *Environment International*, 2, 229–300, [https://doi.org/10.1016/0160-4120\(79\)90005-9](https://doi.org/10.1016/0160-4120(79)90005-9), 1979.
- 460 Keller, K. and Morel, F. M. M.: A model of carbon isotopic fractionation and active carbon uptake in phytoplankton, *Marine Ecology Progress Series*, 182, 295–298, <https://doi.org/10.3354/meps182295>, 1999.
- Key, R. M., Kozyr, A., Sabine, C. L., Lee, K., Wanninkhof, R., Bullister, J. L., Feely, R. A., Millero, F. J., Mordy, C., and Peng, T.-H.: A global ocean carbon climatology: Results from Global Data Analysis Project (GLODAP), *Global Biogeochemical Cycles*, 18, GB4031, 465 <https://doi.org/10.1029/2004GB002247>, 2004.
- Key, R. M., Olsen, A., Van Heuven, S., Lauvset, S. K., Velo, A., Lin, X., Schirnick, C., Kozyr, A., Tanhua, T., Hoppema, M., Jutterstrom, S., Steinfeldt, R., Jeansson, E., Ishi, M., Perez, F. F., and Suzuki, T.: Global Ocean Data Analysis Project, Version 2 (GLODAPv2), ORNL/CDIAC-162, ND-P093, [https://doi.org/10.3334/CDIAC/OTG.NDP093\\_GLODAPv2](https://doi.org/10.3334/CDIAC/OTG.NDP093_GLODAPv2), 2015.
- 470 Köhler, P., Fischer, H., Schmitt, J., and Munhoven, G.: On the application and interpretation of Keeling plots in paleo climate research – deciphering  $\delta^{13}\text{C}$  of atmospheric  $\text{CO}_2$  measured in ice cores, *Biogeosciences*, 3, 539–556, <https://doi.org/10.5194/bg-3-539-2006>, 2006.
- Köhler, P.: Using the Suess effect on the stable carbon isotope to distinguish the future from the past in radiocarbon, *Environmental Research Letters*, 11, 124016, 2016.
- 475 Kutschera, W.: Applications of accelerator mass spectrometry, *International Journal of Mass Spectrometry*, 349–350, 203–218, <https://doi.org/10.1016/j.ijms.2013.05.023>, 2013.
- Large, W. G. and Yeager, S. G.: The global climatology of an interannually varying air–sea flux data set, *Clim Dyn*, 33, 341–364, <https://doi.org/10.1007/s00382-008-0441-3>, 2009. Data obtained from [https://data1.gfdl.noaa.gov/nomads/forms/core/COREv2/CNYF\\_v2.html](https://data1.gfdl.noaa.gov/nomads/forms/core/COREv2/CNYF_v2.html) on 29 June 2021.
- 480 Lauvset, S. K., Key, R. M., Olsen, A., Heuven, S. van, Velo, A., Lin, X., Schirnick, C., Kozyr, A., Tanhua, T., Hoppema, M., Jutterström, S., Steinfeldt, R., Jeansson, E., Ishii, M., Perez, F. F., Suzuki, T., and Watelet, S.: A new global interior ocean mapped climatology: the  $1^\circ \times 1^\circ$  GLODAP version 2, *Earth System Science Data*, 8, 325–340, <https://doi.org/10.5194/essd-8-325-2016>, 2016.
- Laws, E. A., Popp, B. N., Bidigare, R. R., Kennicutt, M. C., and Macko, S. A.: Dependence of 485 phytoplankton carbon isotopic composition on growth rate and  $[\text{CO}_2]_{\text{aq}}$ : Theoretical considerations and experimental results, *Geochimica et Cosmochimica Acta*, 59, 1131–1138, [https://doi.org/10.1016/0016-7037\(95\)00030-4](https://doi.org/10.1016/0016-7037(95)00030-4), 1995.





- Laws, E. A., Bidigare, R. R., and Popp, B. N.: Effect of growth rate and CO<sub>2</sub> concentration on carbon isotopic fractionation by the marine diatom *Phaeodactylum tricornutum*, *Limnology and Oceanography*, 42, 1552–1560, <https://doi.org/10.4319/lo.1997.42.7.1552>, 1997.
- 490
- Liu, B., Six, K. D., and Ilyina, T.: Incorporating the stable carbon isotope <sup>13</sup>C in the ocean biogeochemical component of the Max Planck Institute Earth System Model, *Biogeosciences*, 18, 4389–4429, <https://doi.org/10.5194/bg-18-4389-2021>, 2021.
- Locarnini, R. A., Mishonov, A. V., Antonov, J. I., Boyer, T. P., and Garcia, H. E.: *World Ocean Atlas 2009, Volume 1: Temperature*, Washington, D.C., 2010.
- 495
- Lohmann, G., Butzin, M., Eissner, N., Shi, X., and Stepanek, C.: Abrupt Climate and Weather Changes Across Time Scales, *Paleoceanography and Paleoclimatology*, 35, e2019PA003782, <https://doi.org/10.1029/2019PA003782>, 2020.
- Lorrain, A., Pethybridge, H., Cassar, N., Receveur, A., Allain, V., Bodin, N., Bopp, L., Choy, C. A., Duffy, L., Fry, B., Goni, N., Graham, B. S., Hobday, A. J., Logan, J. M., Ménard, F., Menkes, C. E., Olson, R. J., Pagendam, D. E., Point, D., Revill, A. T., Somes, C. J., and Young, J. W.: Trends in tuna carbon isotopes suggest global changes in pelagic phytoplankton communities, *Global Change Biology*, 26, 458–470, <https://doi.org/10.1111/gcb.14858>, 2020.
- 500
- Lynch-Stieglitz, J., Adkins, J. F., Curry, W. B., Dokken, T., Hall, I. R., Herguera, J. C., Hirschi, J. J.-M., Ivanova, E. V., Kissel, C., Marchal, O., Marchitto, T. M., McCave, I. N., McManus, J. F., Mulitza, S., Ninnemann, U., Peeters, F., Yu, E.-F., and Zahn, R.: Atlantic Meridional Overturning Circulation During the Last Glacial Maximum, *Science*, 316, 66–69, <https://doi.org/10.1126/science.1137127>, 2007.
- 505
- Matsumoto, K., Sarmiento, J. L., Key, R. M., Aumont, O., Bullister, J. L., Caldeira, K., Campin, J.-M., Doney, S. C., Drange, H., Dutay, J.-C., Follows, M., Gao, Y., Gnanadesikan, A., Gruber, N., Ishida, A., Joos, F., Lindsay, K., Maier-Reimer, E., Marshall, J. C., Matear, R. J., Monfray, P., Mouchet, A., Najjar, R., Plattner, G.-K., Schlitzer, R., Slater, R., Swathi, P. S., Totterdell, I. J., Weirig, M.-F., Yamanaka, Y., Yool, A., and Orr, J. C.: Evaluation of ocean carbon cycle models with data-based metrics, *Geophysical Research Letters*, 31, <https://doi.org/10.1029/2003GL018970>, 2004.
- 510
- Menking, J. A., Shackleton, S. A., Bauska, T. K., Buffen, A. M., Brook, E. J., Barker, S., Severinghaus, J. P., Dyonisius, M. N., and Petrenko, V. V.: Multiple carbon cycle mechanisms associated with the glaciation of Marine Isotope Stage 4, *Nat Commun*, 13, 5443, <https://doi.org/10.1038/s41467-022-33166-3>, 2022.
- 515



- Menviel, L., Mouchet, A., Meissner, K. J., Joos, F., and England, M. H.: Impact of oceanic circulation changes on atmospheric  $\delta^{13}\text{C}\text{O}_2$ , *Global Biogeochemical Cycles*, 29, 1944–1961, <https://doi.org/10.1002/2015GB005207>, 2015.
- Morée, A. L., Schwinger, J., Ninnemann, U. S., Jeltsch-Thömmes, A., Bethke, I., and Heinze, C.: Evaluating the biological pump efficiency of the Last Glacial Maximum ocean using  $\delta^{13}\text{C}$ , *Climate of the Past*, 17, 753–774, <https://doi.org/10.5194/cp-17-753-2021>, 2021.
- 525 Mouchet, A., The ocean bomb radiocarbon inventory revisited. *Radiocarbon*, 55, 1580–94, <https://doi.org/10.1017/S0033822200048505>, 2013.
- Munhoven, G.: Model of Early Diagenesis in the Upper Sediment with Adaptable complexity – MEDUSA (v. 2): a time-dependent biogeochemical sediment module for Earth system models, process analysis and teaching, *Geoscientific Model Development*, 14, 3603–3631, <https://doi.org/10.5194/gmd-14-3603-2021>, 2021.
- 530 Orr, J. C., Najjar, R. G., Aumont, O., Bopp, L., Bullister, J. L., Danabasoglu, G., Doney, S. C., Dunne, J. P., Dutay, J.-C., Graven, H., Griffies, S. M., John, J. G., Joos, F., Levin, I., Lindsay, K., Matear, R. J., McKinley, G. A., Mouchet, A., Oeschler, A., Romanou, A., Schlitzer, R., Tagliabue, A., Tanhua, T., and Yool, A.: Biogeochemical protocols and diagnostics for the CMIP6 Ocean Model Intercomparison Project (OMIP), *Geoscientific Model Development*, 10, 2169–2199, <https://doi.org/10.5194/gmd-10-2169-2017>, 2017.
- 535 Popp, B. N., Laws, E. A., Bidigare, R. R., Dore, J. E., Hanson, K. L., and Wakeham, S. G.: Effect of Phytoplankton Cell Geometry on Carbon Isotopic Fractionation, *Geochimica et Cosmochimica Acta*, 62, 69–77, [https://doi.org/10.1016/S0016-7037\(97\)00333-5](https://doi.org/10.1016/S0016-7037(97)00333-5), 1998.
- 540 Quay, P. D., Tilbrook, B., and Wong, C. S.: Oceanic Uptake of Fossil Fuel  $\text{CO}_2$ : Carbon-13 Evidence, 256, 74–79, <https://doi.org/10.1126/science.256.5053.74>, 1992.
- Rafter, P. A., Gray, W. R., Hines, S. K. V., Burke, A., Costa, K. M., Gottschalk, J., Hain, M. P., Rae, J. W. B., Southon, J. R., Walczak, M. H., Yu, J., Adkins, J. F., and DeVries, T.: Global reorganization of deep-sea circulation and carbon storage after the last ice age, *Science Advances*, 8, eabq5434, <https://doi.org/10.1126/sciadv.abq5434>, 2022.
- 545 Rau, G. H., Riebesell, U., and Wolf-Gladrow, D.: A model of photosynthetic  $^{13}\text{C}$  fractionation by marine phytoplankton based on diffusive molecular  $\text{CO}_2$  uptake, *Marine Ecology Progress Series*, 133, 275–285, <https://doi.org/10.3354/meps133275>, 1996.



- Rau, G. H., Riebesell, U., and Wolf-Gladrow, D.: CO<sub>2aq</sub>-dependent photosynthetic <sup>13</sup>C fractionation in  
550 the ocean: A model versus measurements, *Global Biogeochemical Cycles*, 11, 267–278,  
<https://doi.org/10.1029/97GB00328>, 1997.
- Šavrič, B., Patterson, T., and Jenny, B.: The Equal Earth map projection, *International Journal of  
Geographical Information Science*, 33, 454–465, <https://doi.org/10.1080/13658816.2018.1504949>,  
2019.
- 555 Schmittner, A., Gruber, N., Mix, A. C., Key, R. M., Tagliabue, A., and Westberry, T. K.: Biology and  
air–sea gas exchange controls on the distribution of carbon isotope ratios ( $\delta^{13}\text{C}$ ) in the ocean,  
*Biogeosciences*, 10, 5793–5816, <https://doi.org/10.5194/bg-10-5793-2013>, 2013.
- Schmittner, A., Bostock, H. C., Cartapanis, O., Curry, W. B., Filipsson, H. L., Galbraith, E. D.,  
Gottschalk, J., Herguera, J. C., Hoogakker, B., Jaccard, S. L., Lisiecki, L. E., Lund, D. C., Martínez-  
560 Méndez, G., Lynch-Stieglitz, J., Mackensen, A., Michel, E., Mix, A. C., Oppo, D. W., Peterson, C. D.,  
Repschläger, J., Sikes, E. L., Spero, H. J., and Waelbroeck, C.: Calibration of the carbon isotope  
composition ( $\delta^{13}\text{C}$ ) of benthic foraminifera, *Paleoceanography*, 512–530,  
<https://doi.org/10.1002/2016PA003072>, 2017.
- Scholz, P., Sidorenko, D., Gurses, O., Danilov, S., Koldunov, N., Wang, Q., Sein, D., Smolentseva, M.,  
565 Rakowsky, N., and Jung, T.: Assessment of the Finite-volume Sea ice-Ocean Model (FESOM2.0) –  
Part 1: Description of selected key model elements and comparison to its predecessor version.  
*Geoscientific Model Development*, 12, 4875–4899, <https://doi.org/10.5194/gmd-12-4875-2019>, 2019.
- Scholz, P., Sidorenko, D., Danilov, S., Wang, Q., Koldunov, N., Sein, D., and Jung, T.: Assessment of  
the Finite-VolumE Sea ice–Ocean Model (FESOM2.0) – Part 2: Partial bottom cells, embedded sea  
570 ice and vertical mixing library CVMix, *Geoscientific Model Development*, 15, 335–363,  
<https://doi.org/10.5194/gmd-15-335-2022>, 2022.
- Skinner, L. C. and Bard, E.: Radiocarbon as a Dating Tool and Tracer in Paleoceanography, *Reviews of  
Geophysics*, 60, e2020RG000720, <https://doi.org/10.1029/2020RG000720>, 2022.
- Skinner, L. C., Primeau, F., Jeltsch-Thömmes, A., Joos, F., Köhler, P., and Bard, E.: Rejuvenating the  
575 ocean: mean ocean radiocarbon, CO<sub>2</sub> release, and radiocarbon budget closure across the last  
deglaciation, *Clim. Past Discuss.* [preprint], <https://doi.org/10.5194/cp-2023-24>, in review, 2023.
- Steele, M., Morley, R., and Ermold, W.: PHC: A Global Ocean Hydrography with a High-Quality Arctic  
Ocean, *Journal of Climate*, 14, 2079–2087, [https://doi.org/10.1175/1520-0442\(2001\)014<2079:PAGOHW>2.0.CO;2](https://doi.org/10.1175/1520-0442(2001)014<2079:PAGOHW>2.0.CO;2), 2001.
- 580 Stuiver, M. and Polach, H. A.: Discussion; reporting of C-14 data., *Radiocarbon*, 19, 355–363, 1977.



- Suess, H. E.: Radiocarbon Concentration in Modern Wood, *Science*, 122, 415–417, <https://doi.org/10.1126/science.122.3166.415-a>, 1955.
- Tagliabue, A. and Bopp, L.: Towards understanding global variability in ocean carbon-13, *Global Biogeochemical Cycles*, 22, GB1025, <https://doi.org/10.1029/2007GB003037>, 2008.
- 585 Tagliabue, A., Mtshali, T., Aumont, O., Bowie, A. R., Klunder, M. B., Roychoudhury, A. N., and Swart, S.: A global compilation of dissolved iron measurements: focus on distributions and processes in the Southern Ocean, *Biogeosciences*, 9, 2333–2349, <https://doi.org/10.5194/bg-9-2333-2012>, 2012.
- Tjiputra, J. F., Schwinger, J., Bentsen, M., Morée, A. L., Gao, S., Bethke, I., Heinze, C., Goris, N., Gupta, A., He, Y., Oliví, D., Seland, Ø., and Schulz, M.: Ocean biogeochemistry in the Norwegian Earth  
590 System Model version 2 (NorESM2), *Geoscientific Model Development*, 2393–2431, <https://doi.org/10.5194/gmd-13-2393-2020>, 2020.
- Toggweiler, J. R., Dixon, K., Bryan, K.: Simulations of radiocarbon in a coarse-resolution world ocean model: 1. Steady state prebomb distributions, *Journal of Geophysical Research*, 94, 8217–8242, <https://doi.org/10.1029/JC094iC06p08217>, 1989.
- 595 Verwega, M.-T., Somes, C. J., Schartau, M., Tuerena, R. E., Lorrain, A., Oschlies, A., and Slawig, T.: Description of a global marine particulate organic carbon-13 isotope data set, *Earth System Science Data*, 13, 4861–4880, <https://doi.org/10.5194/essd-13-4861-2021>, 2021.
- Wanninkhof, R.: Relationship between wind speed and gas exchange over the ocean revisited: Gas exchange and wind speed over the ocean, *Limnology and Oceanography: Methods*, 12, 351–362,  
600 <https://doi.org/10.4319/lom.2014.12.351>, 2014.
- Young, J. N., Bruggeman, J., Rickaby, R. E. M., Erez, J., and Conte, M.: Evidence for changes in carbon isotopic fractionation by phytoplankton between 1960 and 2010, *Global Biogeochemical Cycles*, 27, 505–515, <https://doi.org/10.1002/gbc.20045>, 2013.
- Zhang, J., Quay, P. D., and Wilbur, D. O.: Carbon isotope fractionation during gas-water exchange and  
605 dissolution of CO<sub>2</sub>, *Geochimica et Cosmochimica Acta*, 59, 107–114, [https://doi.org/10.1016/0016-7037\(95\)91550-D](https://doi.org/10.1016/0016-7037(95)91550-D), 1995.
- Ziveri, P., Stoll, H., Probert, I., Klaas, C., Geisen, M., Ganssen, G., and Young, J.: Stable isotope ‘vital effects’ in coccolith calcite, *Earth and Planetary Science Letters*, 210, 137–149, [https://doi.org/10.1016/S0012-821X\(03\)00101-8](https://doi.org/10.1016/S0012-821X(03)00101-8), 2003.



## Figures

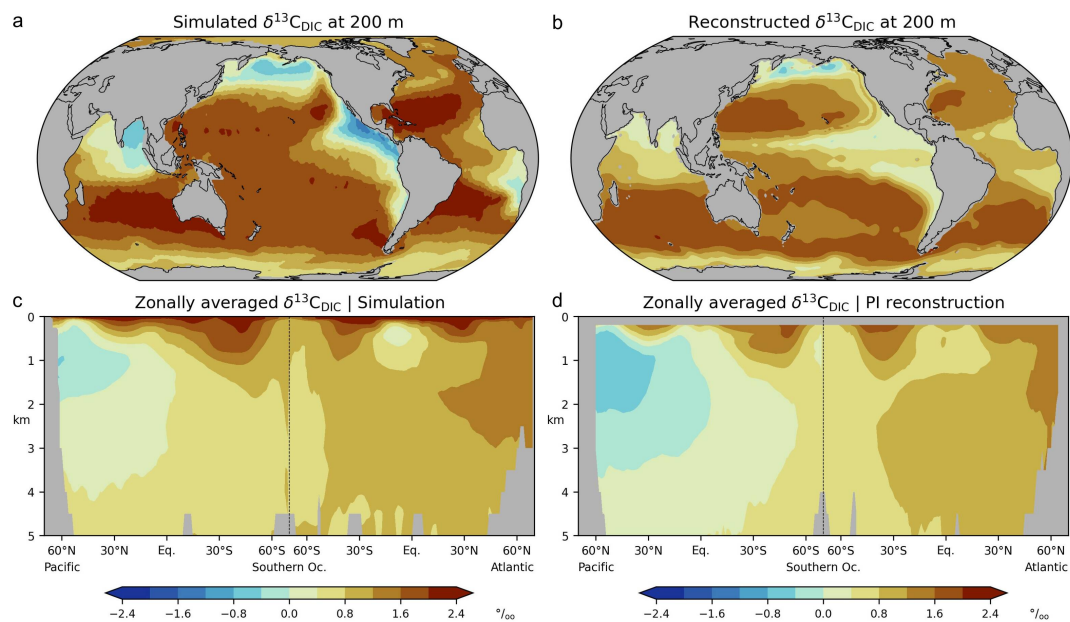
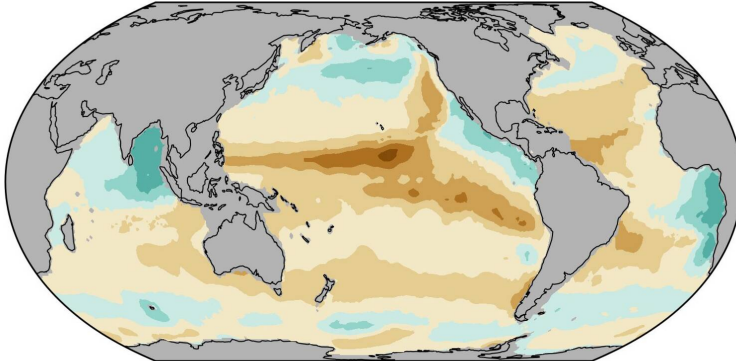


**Figure 1.** Preindustrial  $\delta^{13}\text{C}$  of DIC, (a, c): this study, (b, d): reconstruction (Eide et al., 2017). (a, b):  
615 values at 200 m depth, (c, d) zonal-mean values in the Atlantic and Pacific. Map projection here and in  
other figures is area-preserving (Equal Earth projection, Šavrič et al., 2019)



a  $\delta^{13}\text{C}_{\text{DIC}}$  difference at 200 m | CC - PI reconstruction



b Zonally averaged  $\delta^{13}\text{C}_{\text{DIC}}$  difference | CC - PI reconstruction

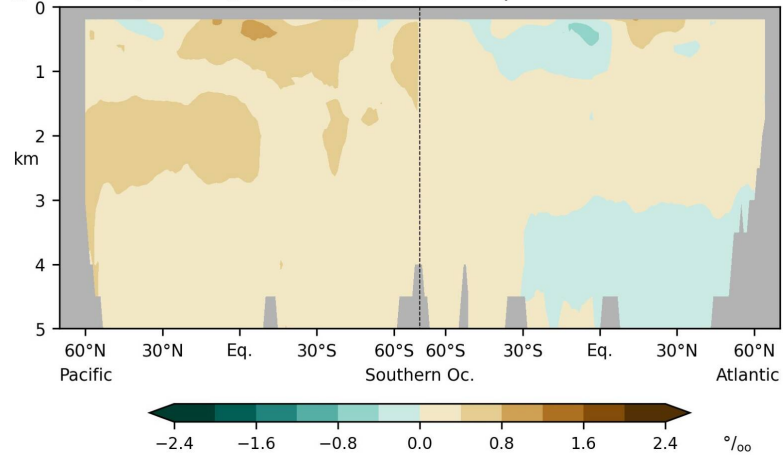


**Figure 2.** Differences between simulated (this study; CC) and reconstructed (Eide et al., 2017; PI)  $\delta^{13}\text{C}$  of DIC for the preindustrial period, (a): at 200 m depth, (b): zonal-mean values in the Atlantic and Pacific.

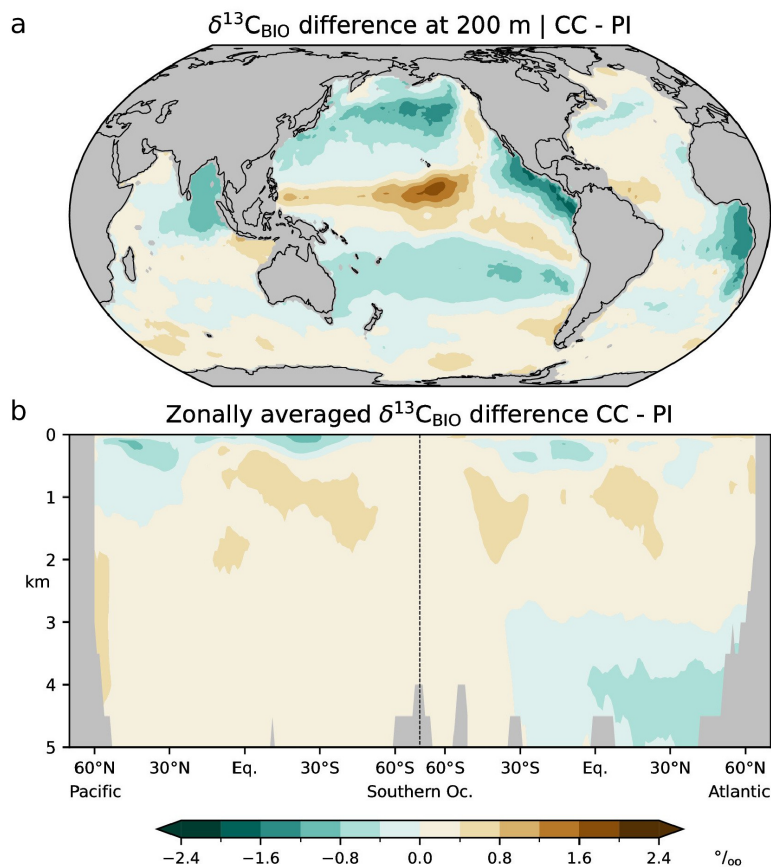


**Figure 3.** Differences between simulated (this study; CC) and estimated (Eide et al., 2017; PI)  $\delta^{13}\text{C}_{\text{BIO}}$  (the biological component of  $\delta^{13}\text{C}_{\text{DIC}}$  in the absence of air-sea exchange) during the preindustrial period, (a): at 200 m depth, (b): zonal-mean values in the Atlantic and Pacific.

625



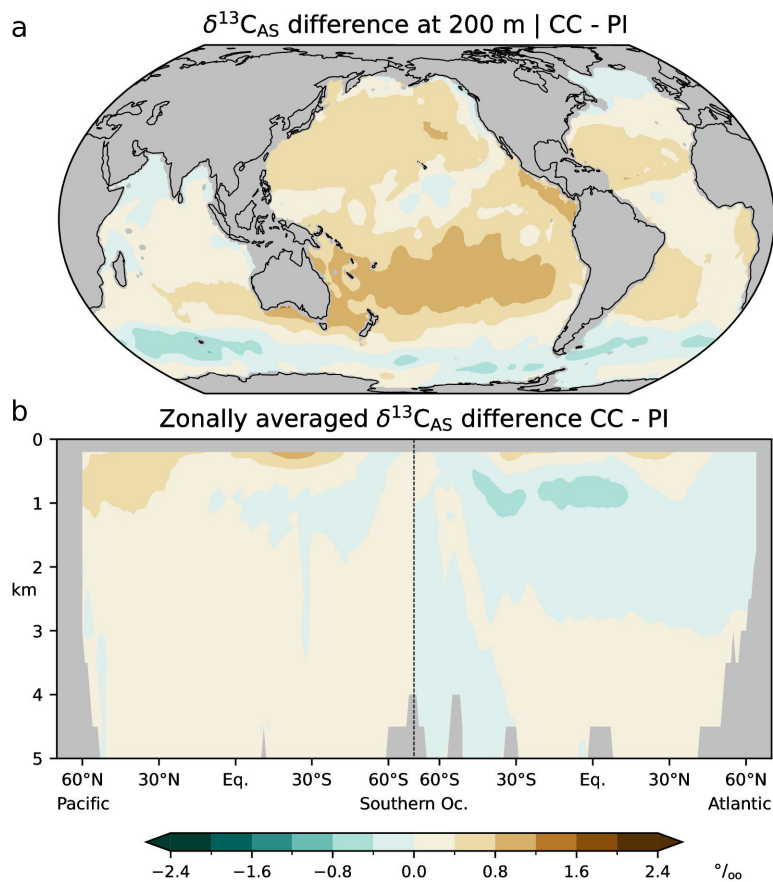


**Figure 4.** Differences between simulated (this study; CC) and estimated (Eide et al., 2017; PI)  $\delta^{13}\text{C}_{\text{AS}} = \delta^{13}\text{C}_{\text{DIC}} - \delta^{13}\text{C}_{\text{BIO}}$  during the preindustrial period, (a): at 200 m depth, (b): zonal-mean values in the  
630 Atlantic and Pacific.

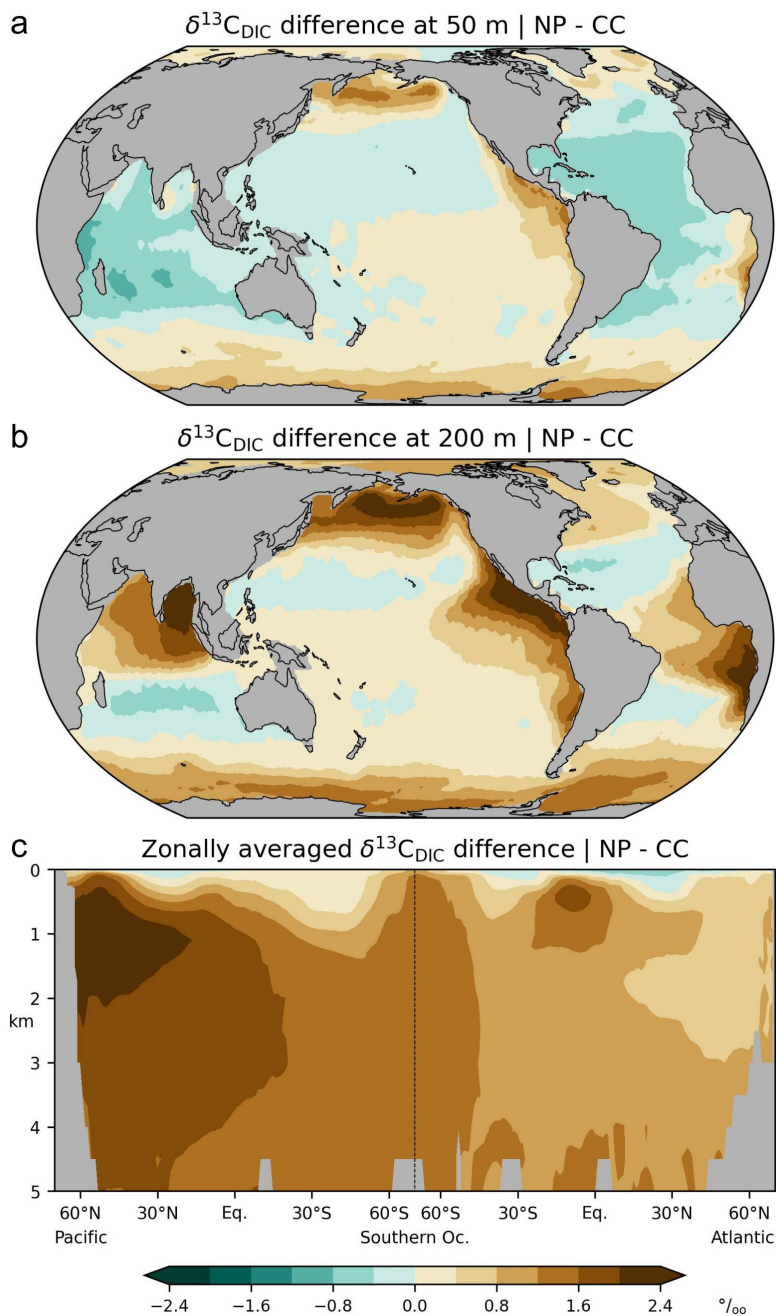


**Figure 5.** Changes in preindustrial  $\delta^{13}\text{C}$  of DIC if isotopic fractionation during photosynthesis is disabled (sensitivity experiment NP versus simulation CC), (a): at 50 m depth, (b) at 200 m depth, (c): zonal-mean values in the Atlantic and Pacific.

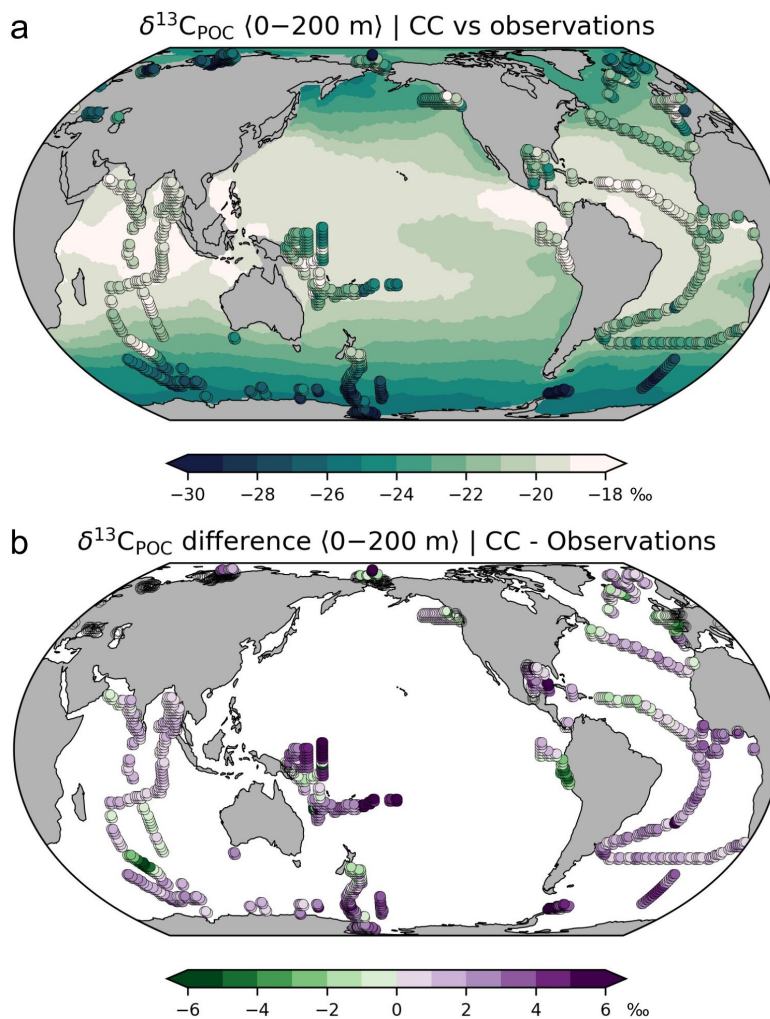
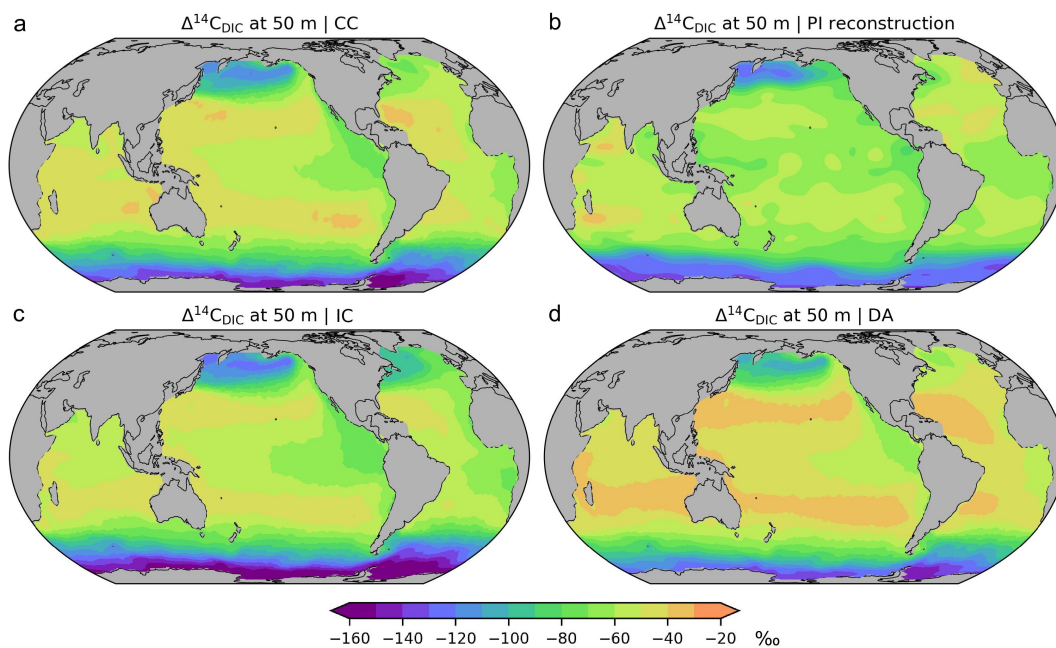
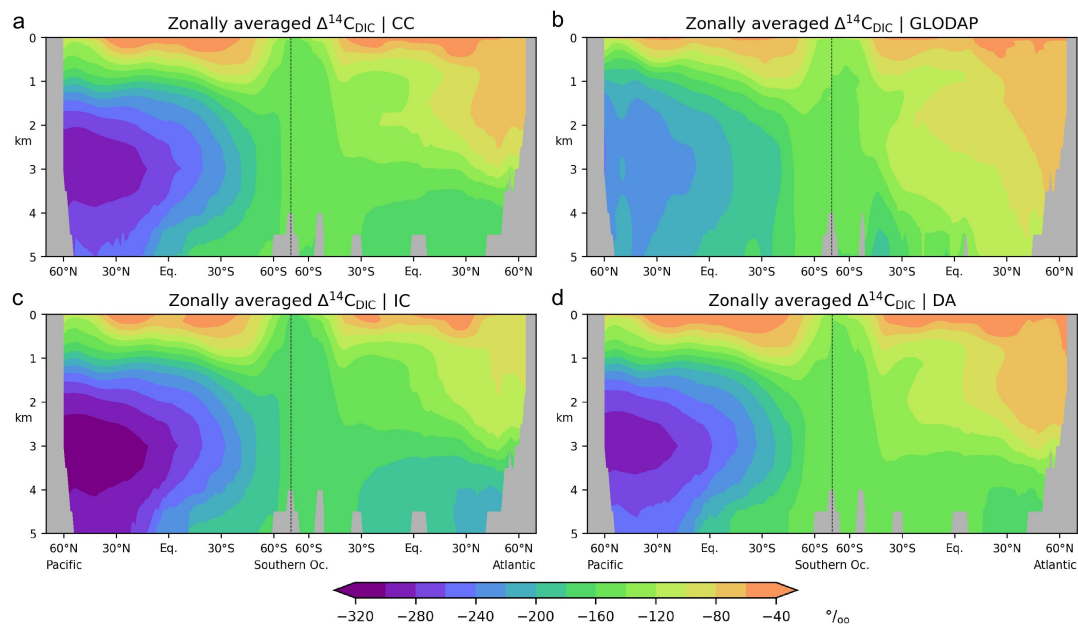


**Figure 6.** (a)  $\delta^{13}\text{C}$  of POC averaged over the upper 200 m. Shaded areas: simulation results (this study),  
640 dots: bulk matter observations for the period 1964-2015 (compilation by Verwega et al., 2021; see further  
references therein). (b) Differences between simulated and observed  $\delta^{13}\text{C}$  of POC.



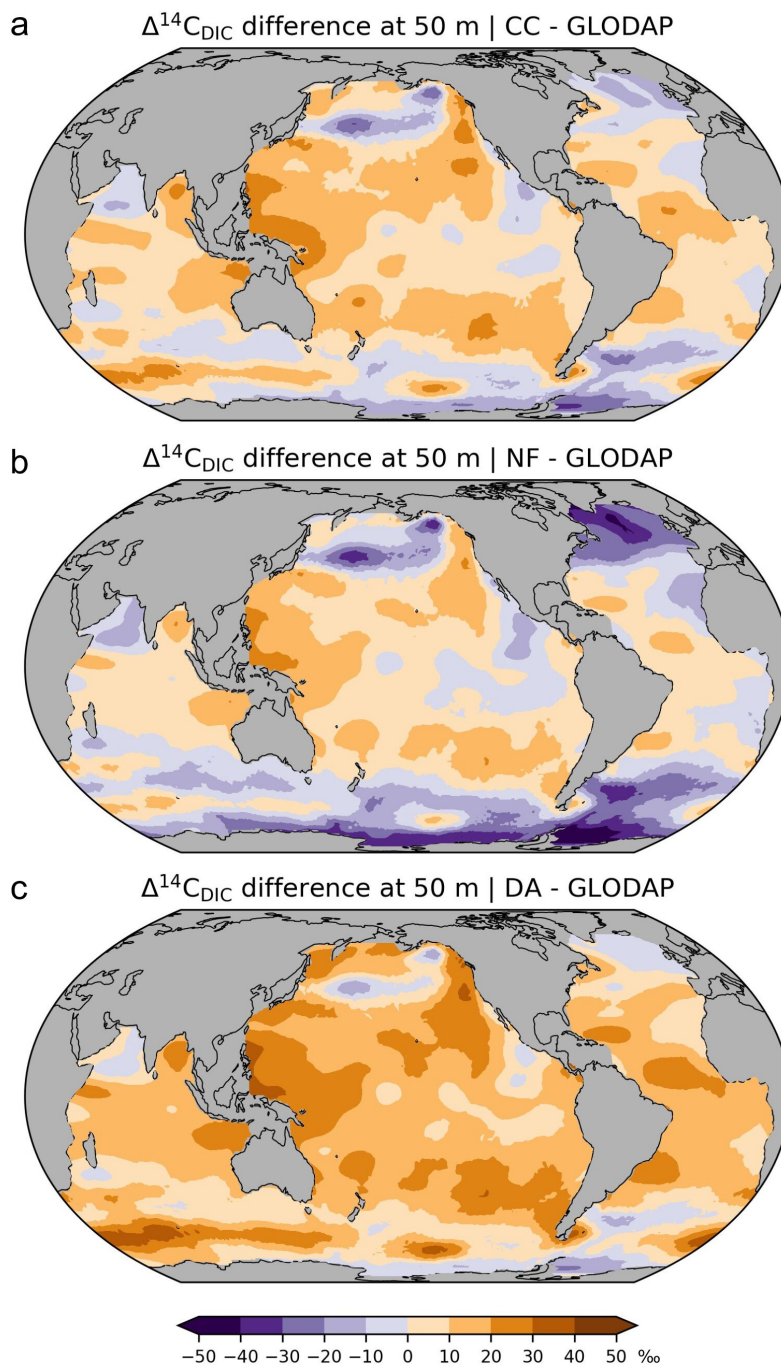
645 **Figure 7.** Preindustrial  $\Delta^{14}\text{C}$  of DIC at 50 m depth, (a): simulation CC considering the complete marine  $^{14}\text{C}$  cycle, (b): reconstruction (Key et al., 2004), (c): simulation IC applying the inorganic  $^{14}\text{C}$  approximation, (d): simulation DA applying the  $\Delta^{14}\text{C}$  approach. See the main text for further explanations.



650

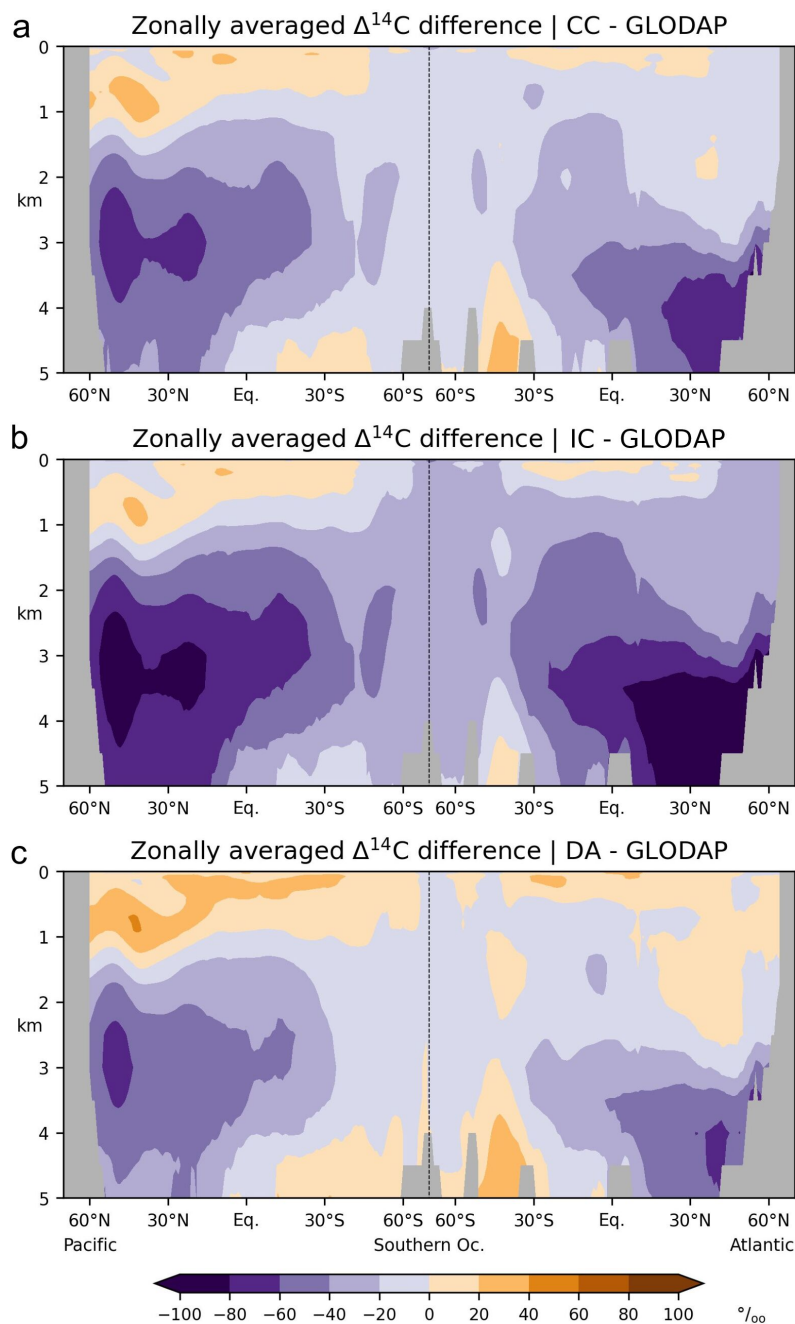
**Figure 8.** Preindustrial  $\Delta^{14}\text{C}$  of DIC in the Atlantic and Pacific. (a): Simulation CC, (b): reconstruction (Key et al., 2004), (c): simulation IC, (d): simulation DA. See the main text for further simulation explanations. Note the different colour scale ranges in Figures 7 and 8.





655

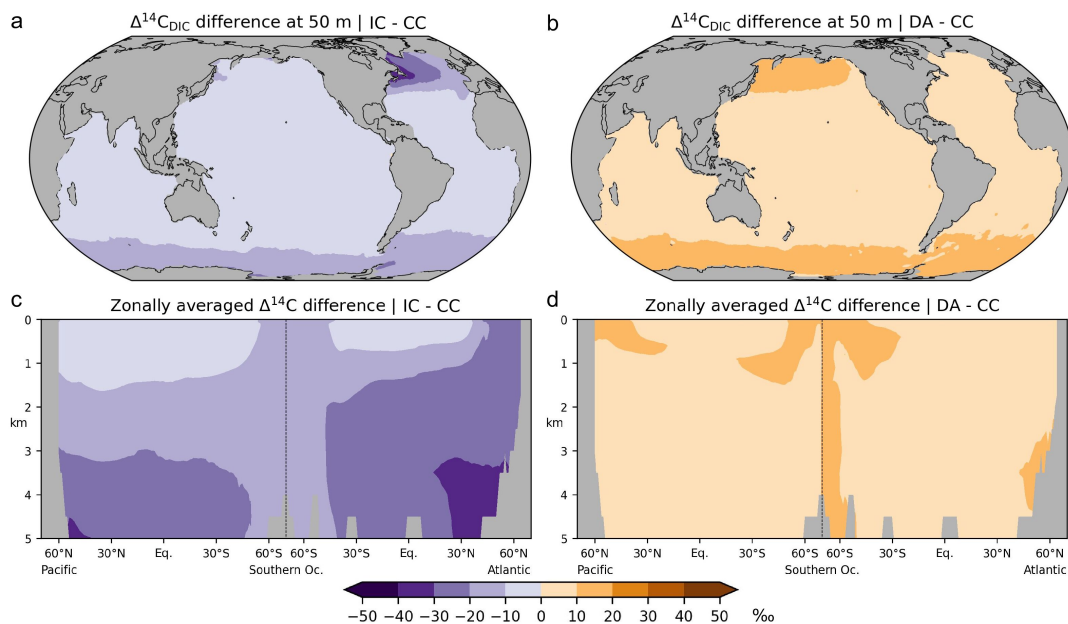
**Figure 9.** Differences between simulated and reconstructed preindustrial  $\Delta^{14}\text{C}$  of DIC at 50 m depth, (a): simulation CC minus reconstruction (GLODAP; Key et al., 2004), (b): simulation IC minus reconstruction, (c): simulation DA minus reconstruction.



660

**Figure 10.** Differences between simulated and reconstructed preindustrial  $\Delta^{14}\text{C}$  of DIC in the Atlantic and Pacific, shown are zonal-mean values, (a): simulation CC minus reconstruction (GLODAP; Key et al., 2004), (b): simulation IC minus reconstruction, (c): simulation DA minus reconstruction. Note the different colour scale ranges in Figures 9 and 10.





665

**Figure 11.** Absolute differences in preindustrial  $\Delta^{14}\text{C}_{\text{DIC}}$  between the various simulation approaches, shown are results at 50 m depth (a, b) and in the Atlantic and Pacific (c, d). (a, c): Inorganic  $^{14}\text{C}$  (IC) modelling approach versus complete  $^{14}\text{C}$  cycle (CC), (b, d):  $\Delta^{14}\text{C}$  approximation (DA) versus simulation

670 CC.

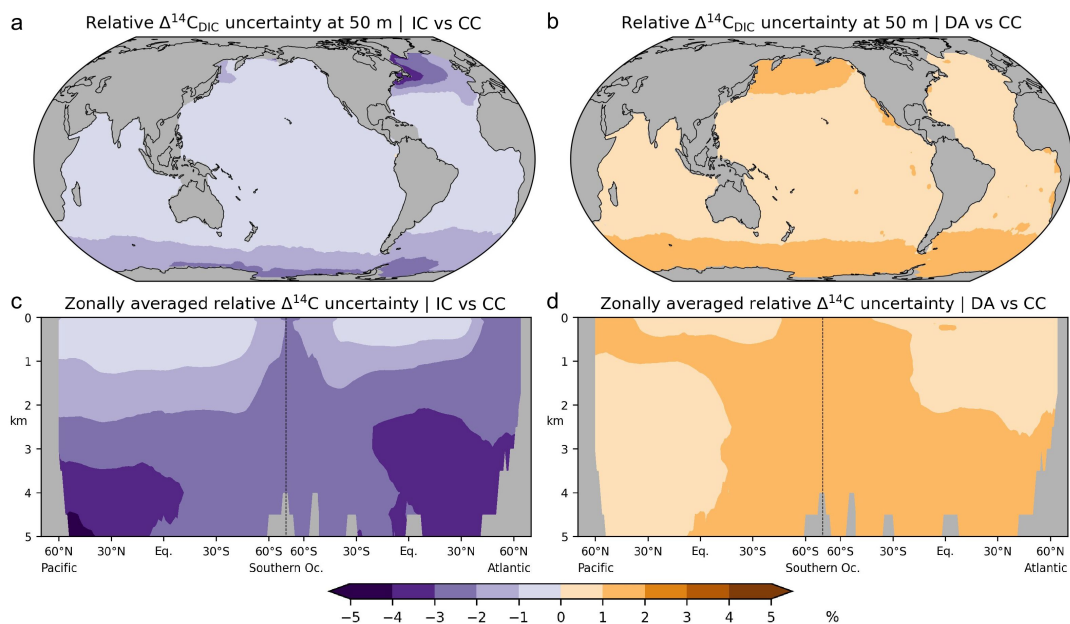


**Figure 12.** Relative differences in preindustrial  $\Delta^{14}\text{C}_{\text{DIC}}$  between the various simulation approaches, 675 shown are absolute values at 50 m depth (a, b) and in the Atlantic and Pacific (c, d). (a, c): No-fractionation (IC) approach versus complete  $^{14}\text{C}$  cycle (CC), (b, d):  $\Delta^{14}\text{C}$  approximation (DA) versus simulation CC.



## Table

**Table 1.** List of model experiments discussed in this paper.

| Name | Description                                     | $^{13}\text{C}$ | $^{14}\text{C}$  | Notes  |
|------|---|-----------------|--|--|
| CC   | Complete $^{14}\text{C}$ cycle                  | Yes             | DI $^{14}\text{C}$<br>DO $^{14}\text{C}$<br>PI $^{14}\text{C}$<br>PO $^{14}\text{C}$ | Control experiment   |
| IC   | Inorganic $^{14}\text{C}$ only                  | Yes             | DI $^{14}\text{C}$   | Isotopic fractionation of $^{14}\text{C}$ is also neglected        |
| NP   | No isotopic fractionation during photosynthesis | Yes             | As in IC   | Sensitivity experiment to study $\delta^{13}\text{C}_{\text{DIC}}$ |
| DA   | $\Delta^{14}\text{C}$ approximation             | No              | $\Delta^{14}\text{C}_{\text{DIC}}$   | Without REcoM3, only FESOM2.1                                      |



## 680 Appendix A

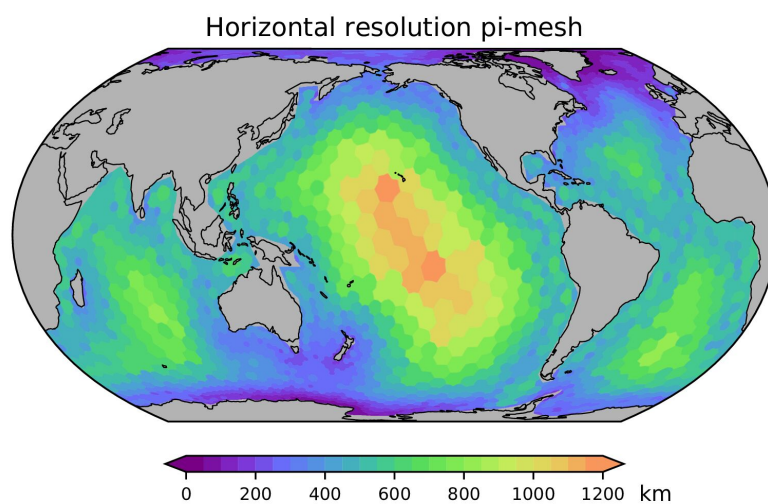


**Figure A1.** Horizontal resolution of FESOM2.1-REcoM used in this study. The mesh has 3140 surface nodes. See also <https://fesom.de/models/meshesetups/> for an impression of the bathymetry.

685

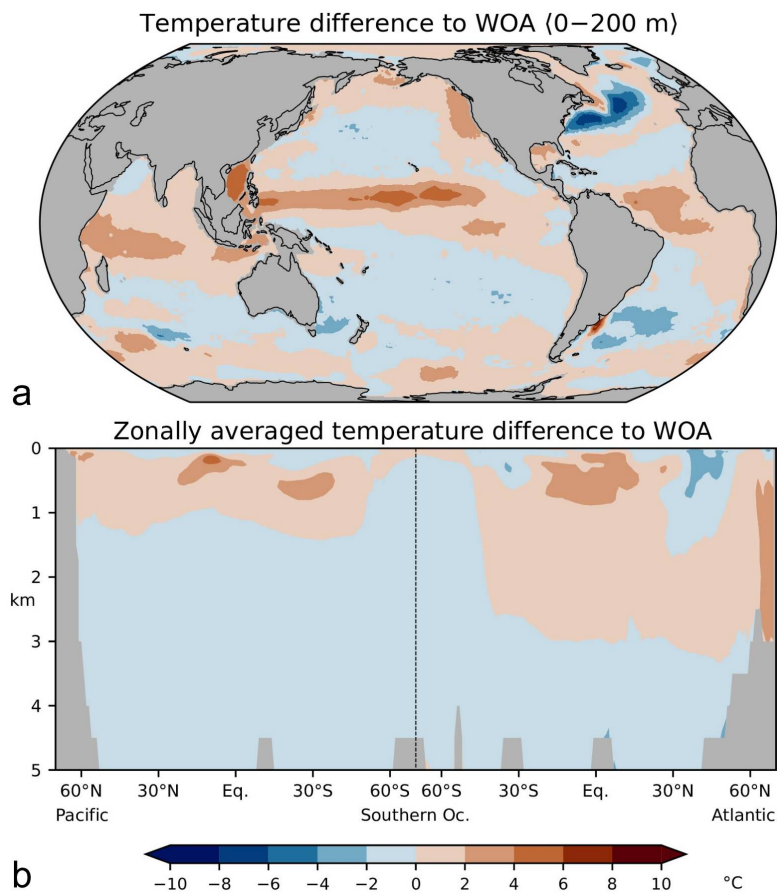


**Figure A2.** Differences between simulated and observed (Locarnini et al., 2010) temperatures, (a) averaged over the upper 200 m, (b) in the Atlantic and Pacific. See Scholz et al. (2019) for comparison  
690 with higher-resolution simulations.

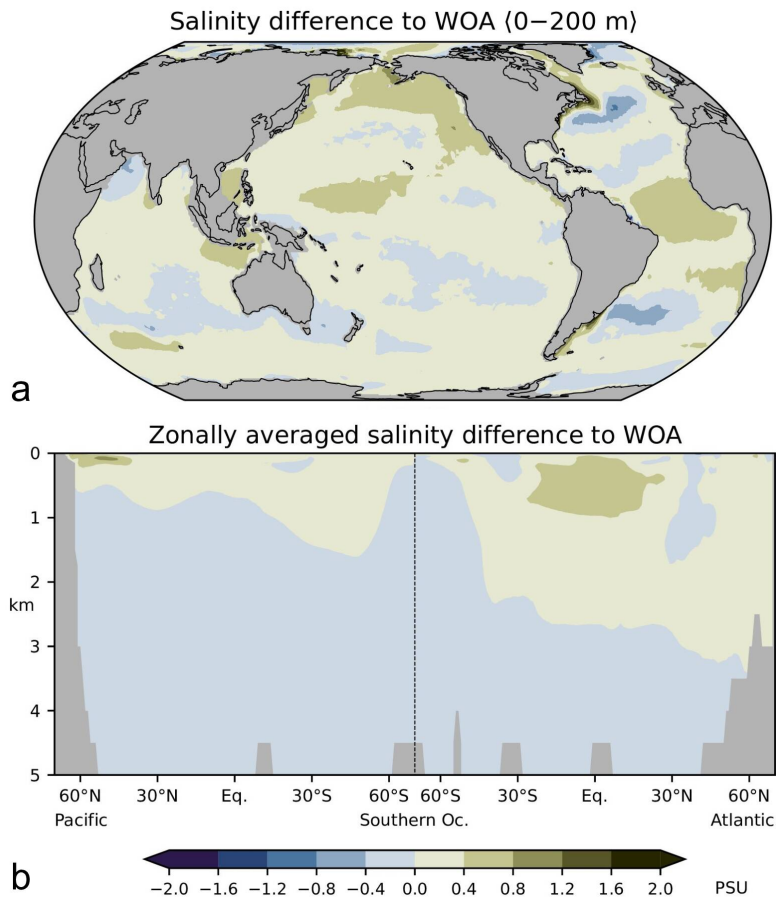


**Figure A3.** Differences between simulated and observed (Antonov et al., 2010) salinities, (a) averaged  
695 over the upper 200 m, (b) in the Atlantic and Pacific. See Scholz et al. (2019) for comparison with higher-  
resolution simulations.

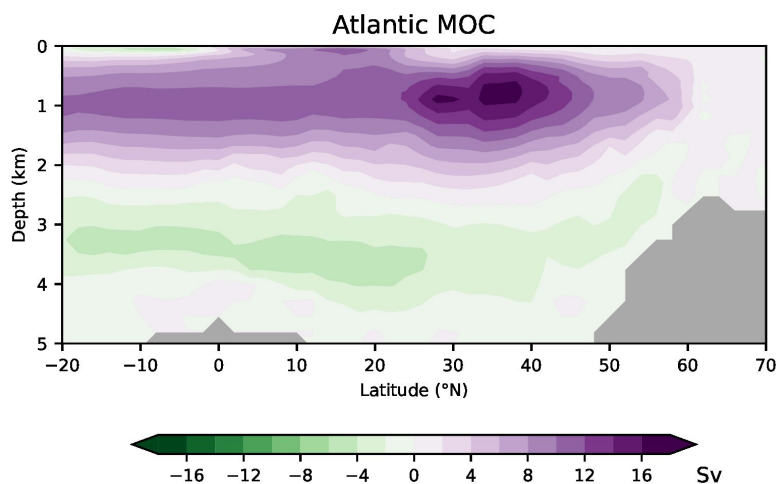


**Figure A4.** Simulated meridional overturning circulation (MOC,  $1 \text{ Sv} = 1 \times 10^6 \text{ m}^3 \text{ s}^{-1}$ ) in the Atlantic.  
700 See also Scholz et al. (2019, 2022) for comparison with higher-resolution simulations.

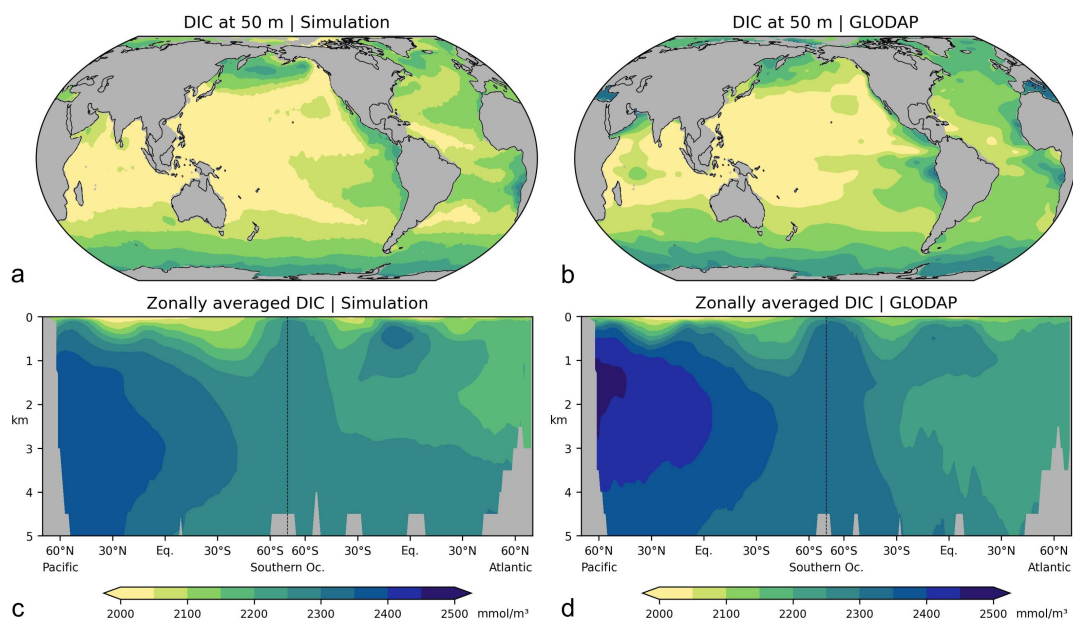


**Figure A5.** Concentrations of dissolved inorganic carbon (DIC), (a, c): this study, (b, d): observations for 1972 - 2013 CE, normalized to the year 2002 (Key et al., 2015; Lauvset et al., 2016). (a, b): Concentrations at 50 m depth, (c, d) zonal-mean values in the Atlantic and Pacific. Model results are interpolated to the resolution of the observations ( $1^\circ \times 1^\circ \times 33$  layers).